

Variational partition-of-unity localizations of space-time dual weighted residual estimators for parabolic problems

J.P. Thiele¹ and T. Wick^{1,2,3}

¹Leibniz University Hannover, Institute of Applied Mathematics, Scientific Computing
Welfengarten 1, 30167 Hannover, Germany

²Cluster of Excellence PhoenixD (Photonics, Optics, and Engineering - Innovation Across
Disciplines), Leibniz University Hannover, Germany

³Université Paris-Saclay, LMPS - Laboratoire de Mécanique Paris-Saclay, 91190
Gif-sur-Yvette, France

Abstract

In this work, we consider space-time goal-oriented a posteriori error estimation for parabolic problems. Temporal and spatial discretizations are based on Galerkin finite elements of continuous and discontinuous type. The main objectives are the development and analysis of space-time estimators, in which the localization is based on a weak form employing a partition-of-unity. The resulting error indicators are used for temporal and spatial adaptivity. Our developments are substantiated with several numerical examples.

1 Introduction

Space-time methods for solving differential equations with Galerkin-type finite element methods go back to [46] and a recent state-of-the-art summary was compiled in [37]. Space-time methods can be divided into two categories: the numerical solution and error estimation. In this work, we are primarily interested in the latter. After the previously mentioned early work, various problems have been considered in space-time formulations such as incompressible flow [56], first-order hyperbolic systems [12], elastic wave equation [28, 29, 31], visco-acoustic/visco-elastic wave equations [13], financial mathematics [25], the Biot equations in poroelasticity [5], and fluid-structure interaction [27, 58, 59, 57, 55, 23]. Advancements for the numerical solution by means of space-time methods, such as for example multi-grid methods, were undertaken in [45, 24, 50] and with space-time domain decomposition [53].

Classical norm-based a posteriori error estimation was done for parabolic problems in [18, 19, 62, 54, 34, 36]. Goal-oriented error estimation of space-time problems was performed in [40, 52, 51, 9]. Therein, space-time formulations may serve three purposes: spatial error estimation, temporal error estimation [41, 42, 23, 25] or both simultaneously [52, 51, 3, 9, 12, 13]. Decoupling space and time for rate-dependent problems in elasto-plasticity was considered in [47]. Moreover, we mention space-time developments in PDE-based optimization with and without a posteriori error control [40, 6, 43,

44, 22, 21, 39, 38, 35, 30]. A brief review of space-time concepts for goal-oriented a posteriori error estimation in fluid-structure interaction for deriving the adjoint in goal-oriented error estimation and optimization was conducted in [63].

Employing the dual-weighted residual method [7, 8] for space-time goal-oriented error estimation comes with the challenge that the adjoint problem is running backwards-in-time. For nonlinear problems, this means that the primal solution must be available at the respective time points. This can be done by simply storing all primal solutions in the RAM (random access memory) or hard disk, or by using checkpointing techniques [51, 40].

The main objective in this work is to combine space-time concepts from [52] with an easy-to-implement partition-of-unity localization proposed in [49]. The latter was established for stationary problems, which is extended in this study to space-time error estimation. Two error estimators are proposed: joint and split. Because of Galerkin orthogonality, we need higher-order information in the adjoint problem for calculation of the primal residual estimator. There are different ways to achieve this. For stationary problems a mixed order approach is often used. There, we discretize the primal problem with the low order $cG(s)dG(r)$ elements and the adjoint problem with high order $cG(s+1)cG(r+1)$ elements. The notation was proposed in [20, 17] and means that spatial discretization is based on $cG(s)$ or $cG(s+1)$ continuous Galerkin finite elements respectively, where $s \in \mathbb{N}_0$ indicates the polynomial degree, while temporal discretization is based on $dG(r)$, discontinuous Galerkin finite elements, where $r \in \mathbb{N}_0$ indicates the temporal polynomial degree. In the case of $cG(r+1)$ the trial functions are continuous, while the test functions are still discontinuous and of order r .

This approach needs interpolation operators to calculate the low order adjoint solution. In the equal low order approach both problems are discretized with low order elements and the high order solutions are obtained by a suitable patch wise reconstruction operator. For the adjoint estimator higher-order information in the primal problem is needed as well. For the two earlier approaches this can again be calculated by patch wise reconstruction. Alternatively, in the equal high order approach both problems can be discretized with high order elements. Then, only interpolation operators are needed but the whole solution becomes more expensive. Additionally, these approaches can be mixed by using different approaches for temporal and spatial discretization.

From the resulting a posteriori error estimates, local error indicators are extracted to establish adaptive algorithms for both temporal and spatial mesh refinement. For verification, error reductions and effectivity indices are observed. Finally, we establish some theoretical results by extending the two-sided error estimates from [15, 14] to space-time settings. Assuming a space-time saturation assumption on the goal-functional, this extension is formally straightforward, but care has to be taken with the choice of the function spaces. These details are worked out in this paper.

Some preliminary results were published in the conference proceedings papers [61] (heat equation) and [60] (low mach number combustion). However, technical derivations and the theory have not been worked out therein. Moreover, the current work provides (for the first time) detailed computational comparisons of the joint and split error estimators in terms of effectivity indices as well as thorough investigations of the PU-DWR method in a space-time context. Additionally, we look at a proof-of-

concept for fully anisotropic space-time grid refinement.

The outline of this paper is as follows: In Section 2, the primal problem statements are provided including their space-time discretizations. Next, in Section 3, the dual-weighted residual method is recapitulated. Afterward in Section 4, partition-of-unity DWR space-time goal-oriented a posteriori error estimators are proposed. In Section 5, four numerical examples are studied in order to substantiate our algorithmic developments. We summarize our work in Section 6.

2 Space-time notation and problem formulations

The space time domain is denoted by $\Sigma \subset \mathbb{R}^{d+1}$ with $\Sigma = \{\Omega(t) \subset \mathbb{R}^d : t \in I\}$, with the temporal interval $I = (0, T)$ and spatial domain Ω . In this paper, we consider time-independent domains Ω , resulting in $\Sigma = \Omega \times I$.

Using $V = H^1(\Omega)$ and $H = L^2(\Omega)$ we can define our space-time Hilbert space as

$$X := W(0, T) := \{v : v \in L^2(I, V) \text{ and } \partial_t v \in L^2(I, V^*)\} \quad (1)$$

with scalar product

$$(u, v) := (u, v)_{L^2(I, H)} = \int_0^T (u(t), v(t))_H dt. \quad (2)$$

Furthermore, let $A : X \times X \rightarrow \mathbb{R}$ be a semi-linear form, being nonlinear in the first argument and linear in the second argument. Let $F : X \rightarrow \mathbb{R}$ be a linear form representing given right hand side data.

2.1 Discretization

In principle, the discretization steps are the same for all parabolic problems. Since we want to be able to have different trial functions in time and space, we split the discretization, starting with the temporal derivatives. For this we decompose the closure of the time interval into M subintervals $\bar{I} = \{0\} \cup I_1 \cup \dots \cup I_M$, with half-open $I_m := (t_{m-1}, t_m]$. On this triangulation we can define two semidiscrete spaces for a given polynomial degree $r \in \mathbb{N}_0$. We follow [52] for the definition of the function spaces:

$$X_k^r := \{v_k \in C(\bar{I}, H) : v_k|_{I_m} \in \mathcal{P}_r(I_m, V)\}, \quad (3)$$

$$\tilde{X}_k^r := \{v_k \in L^2(\bar{I}, H) : v_k|_{I_m} \in \mathcal{P}_r(I_m, V) \text{ and } v_k(0) \in H\}. \quad (4)$$

In contrast to X_k^r , functions in \tilde{X}_k^r are allowed to have discontinuities at the subinterval endpoints. There we also define the limits from above and below as $v_{k,m}^\pm := \lim_{\varepsilon \rightarrow 0} v_k(t_m \pm \varepsilon)$ and the jump across temporal intervals as $[v_k]_m := v_{k,m}^+ - v_{k,m}^-$.

With $A(u_k)(\varphi)$ and $F(\varphi)$ depending on the actual problem, the general time-discrete weak $dG(r)$ formulations read: Find $u_k \in \tilde{X}_k^r$, where $r \geq 0$, such that

$$A(u_k)(\varphi_k) = F(\varphi_k) \quad \forall \varphi_k \in \tilde{X}_k^r. \quad (5)$$

The general time-discrete weak $cG(r)$ formulation reads as: Find $u_k \in X_k^r$, where $r \geq 1$, such that

$$A(u_k)(\varphi_k) = F(\varphi_k) \quad \forall \varphi_k \in \tilde{X}_k^{r-1}. \quad (6)$$

For continuous trial functions the jump terms in $A(u_k)(\varphi_k)$ vanish.

Remark 2.1. *Due to the directionality of the temporal axis (i.e. $u(t_1)$ independent of $u(t_2)$ for $t_2 > t_1$), the problem could also be split into n subproblems with $T_0 = 0 < T_1 < \dots < T_n = T$. Then, we would have $u(t) = u_i(t)$ for $t \in (T_{i-1}, T_i]$. The subproblem for the heat equation reads as:*

$$\begin{aligned} \partial_t u_i - \Delta u_i &= f(t) \text{ in } \Omega \times (T_{i-1}, T_i) \\ u_i(T_{i-1}, x) &= u_{i-1}(T_{i-1}, x) \text{ in } \Omega \\ u_i(t, x) &= u_D(t, x) \text{ on } \partial\Omega \times (T_{i-1}, T_i) \end{aligned}$$

with $u_0(t, x)$ as the given initial conditions. So strictly speaking, discontinuous test functions for the $cG(r)$ discretization would not be necessary, but simplify the derivations greatly. With $cG(r)$ elements we have $1 + rM$ temporal DoFs and with $dG(r)$ we have $(r + 1)M$ DoFs, so using discontinuous test functions of lower order in time yields approximately the same number of temporal DoFs for test and trial functions.

For the spatial discretization we use triangulations \mathcal{T}_h^m of Ω , where $m = 1, \dots, M$ indicates each temporal subinterval I_m . These are decomposed into quadrilateral/hexagonal elements K and we use continuous test and trial functions of degree s resulting in $V_h^s \subset V$ defined as

$$V_h^{s,m} := \{v_h \in V : v_h|_K \in Q_s(K) \forall K \in \mathcal{T}_h^m\}. \quad (7)$$

Remark 2.2. *Note that we can have different triangulations on different subintervals, resulting in time-dependent or dynamic meshes.*

Using this, we can define the fully discrete function spaces $X_{k,h}^{r,s}$ and $\tilde{X}_{k,h}^{r,s}$:

$$\begin{aligned} X_{k,h}^{r,s} &:= \{v_{kh} \in C(\bar{I}, H) \mid v_{kh}|_{I_m} \in X_{k,h}^{r,s,m}\} \\ \tilde{X}_{k,h}^{r,s} &:= \{v_{kh} \in L^2(I, V) \mid v_{kh}|_{I_m} \in P_r(I_m, V_h^{s,m}) \text{ and } v_{kh}(0) \in V_h^{s,0}\}, \end{aligned}$$

where $X_{k,h}^{r,s,m} \subset P_r(I_m, V)$ and for more details, we refer the reader to [52].

Remark 2.3. *We have the following properties:*

$$\begin{aligned} X_{k,h}^{r,s} &\subset X_k^r \subset X \\ \tilde{X}_{k,h}^{r,s} &\subset \tilde{X}_k^r \not\subset X, & \tilde{X}_{k,h}^{r,s} &\subset \tilde{X}_k^r \subset X + \tilde{X}_k^r \\ X_k^r &\subset X_k^{r+1}, & X_{k,h}^{r,s} &\subset X_{k,h}^{r+1,s+1} \\ \tilde{X}_k^r &\subset \tilde{X}_k^{r+1}, & \tilde{X}_{k,h}^{r,s} &\subset \tilde{X}_{k,h}^{r+1,s+1} \end{aligned}$$

We notice that X is a dense subspace of $X + \tilde{X}_k^r$, which is important for the validity of the theoretical results that follow in Section 3.2 and Section 3.3.

Inserting the appropriate trial- and test-functions we obtain the fully discrete $cG(s)dG(r)$ formulation: Find $u_{kh} \in \tilde{X}_{k,h}^{r,s}$, such that

$$A(u_{kh})(\varphi_{kh}) = F(\varphi_{kh}) \quad \forall \varphi_{kh} \in \tilde{X}_{k,h}^{r,s}, \quad (8)$$

as well as the $cG(s)cG(r)$ formulation: Find $u_{kh} \in X_{k,h}^{r,s}$, such that

$$A(u_{kh})(\varphi_{kh}) = F(\varphi_{kh}) \quad \forall \varphi_{kh} \in \tilde{X}_{k,h}^{r-1,s}. \quad (9)$$

2.2 Heat equation

Let $u : \Sigma \rightarrow \mathbb{R}$ be the solution of the heat equation

$$\partial_t u - \Delta u = f \text{ in } \Sigma, \quad (10)$$

$$u = 0 \text{ on } \partial\Omega \times I,$$

$$u = u^0 \text{ on } \Omega \times \{t = 0\},$$

for a given initial condition $u^0 \in H$ and right hand side function $f \in L^2(0, T; V^*)$.

Using the discretization steps as described above, we obtain the following equations

$$\begin{aligned} A_{\text{heat}}(u_{kh})(\varphi_{kh}) &:= \sum_{m=1}^M \int_{I_m} (\partial_t u_{kh}, \varphi_{kh})_H dt + (\nabla u_{kh}, \nabla \varphi_{kh}) \\ &\quad + \sum_{m=0}^{M-1} ([u_{kh}]_m, \varphi_{kh,m}^+)_H + (u_{kh,0}^-, \varphi_{kh,0}^-)_H \end{aligned} \quad (11)$$

$$F_{\text{heat}}(\varphi_{kh}) := (f, \varphi_{kh}) + (u^0, \varphi_{kh,0}^-)_H. \quad (12)$$

2.3 Combustion

The following coupled nonlinear PDE describes the temperature dependent reaction and diffusion of a combustible substance without the influence of an additional fluid flow ($v \equiv 0$); see [33]. Therefore, the low mach number hypothesis holds and the fluid flow is not influenced by the reaction and can be ignored. The resulting equations for the dimensionless temperature $\theta : \Sigma \rightarrow \mathbb{R}$ and the species concentration $Y : \Sigma \rightarrow \mathbb{R}$ are

$$\partial_t \theta - \Delta \theta = \omega(\theta, Y) \text{ in } \Sigma, \quad (13)$$

$$\partial_t Y - \frac{1}{Le} \Delta Y = -\omega(\theta, Y) \text{ in } \Sigma, \quad (14)$$

with the combustion reaction described by Arrhenius law

$$\omega(u) := \omega(\theta, Y) := \frac{\beta^2}{2Le} Y \exp\left(\frac{\beta(\theta - 1)}{1 + \alpha(\theta - 1)}\right). \quad (15)$$

The Arrhenius law is parametrized by the Lewis number $Le > 0$, the gas expansion $\alpha > 0$ and the dimensionless activation energy $\beta > 0$.

We want to be able to allow all three common types of boundary conditions i.e. those of Dirichlet, Neumann and Robin type. For this we split the boundary $\partial\Omega$ into three non-overlapping parts Γ_D ,

Γ_N and Γ_R . The Dirichlet boundary conditions are built into the function spaces, which is the usual approach. The Neumann and Robin boundary conditions are given by

$$\partial_n \theta = g_N^\theta \text{ on } \Gamma_N \times I \quad (16)$$

$$\partial_n Y = g_N^Y \text{ on } \Gamma_N \times I \quad (17)$$

$$a_R^\theta \theta + b_R^\theta \partial_n \theta = g_R^\theta \text{ on } \Gamma_R \times I \quad (18)$$

$$a_R^Y Y + b_R^Y \partial_n Y = g_R^Y \text{ on } \Gamma_R \times I. \quad (19)$$

It remains to state the initial conditions:

$$\theta = \theta^0 \quad \text{on } \Omega \times \{t = 0\},$$

$$Y = Y^0 \quad \text{on } \Omega \times \{t = 0\}.$$

By following the typical steps for the derivation of a weak formulation, integration by parts in space, and subsequent summation, we obtain

$$\begin{aligned} & (\partial_t \theta, \varphi^\theta) + (\nabla \theta, \nabla \varphi^\theta) - \int_{I \times \partial \Omega} \partial_n \theta \varphi^\theta \, ds dt - (\omega(\theta, Y), \varphi^\theta) \\ & + (\partial_t Y, \varphi^Y) + (\nabla Y, \nabla \varphi^Y) - \int_{I \times \partial \Omega} \partial_n Y \varphi^Y \, ds dt + (\omega(\theta, Y), \varphi^Y) = 0. \end{aligned}$$

Splitting the boundary integrals and considering homogeneous Dirichlet conditions on some parts, i.e., $\varphi^\theta|_{\Gamma_D} = \varphi^Y|_{\Gamma_D} = 0$, we get

$$\int_{I \times \partial \Omega} \partial_n \theta \, ds dt = \int_{I \times \Gamma_N} g_N^\theta \varphi^\theta \, ds dt + \int_{I \times \Gamma_R} \frac{g_R^\theta}{b_R^\theta} \varphi^\theta - \frac{a_R^\theta}{b_R^\theta} \theta \varphi^\theta \, ds dt, \quad (20)$$

$$\int_{I \times \partial \Omega} \partial_n Y \, ds dt = \int_{I \times \Gamma_N} g_N^Y \varphi^Y \, ds dt + \int_{I \times \Gamma_R} \frac{g_R^Y}{b_R^Y} \varphi^Y - \frac{a_R^Y}{b_R^Y} Y \varphi^Y \, ds dt. \quad (21)$$

By introducing jump terms as described earlier, we obtain the following semi-linear and linear forms, respectively:

$$\begin{aligned} A_{\text{comb.}}(u_{kh})(\varphi_{kh}) &:= \sum_{m=1}^M \int_{I_m} (\partial_t \theta_{kh}, \varphi_{kh}^\theta)_H \, dt + ([\theta_{kh}]_{m-1}, \varphi_{kh,m-1}^{\theta,+})_H + (\nabla \theta_{kh}, \nabla \varphi_{kh}^\theta) \\ &+ \sum_{m=1}^M \int_{I_m} (\partial_t Y_{kh}, \varphi_{kh}^Y)_H \, dt + ([Y_{kh}]_{m-1}, \varphi_{kh,m-1}^{Y,+})_H + (\nabla Y_{kh}, \nabla \varphi_{kh}^Y) \\ &+ \int_{I \times \Gamma_R} \frac{a_R^\theta}{b_R^\theta} \theta \varphi^\theta + \frac{a_R^Y}{b_R^Y} Y \varphi^Y \, ds dt + (\omega(u_{kh}), \varphi_{kh}^Y - \varphi_{kh}^\theta) \\ &+ (\theta_{kh,0}^-, \varphi_{kh,0}^{\theta,-})_H + (Y_{kh,0}^-, \varphi_{kh,0}^{Y,-})_H, \end{aligned} \quad (22)$$

$$\begin{aligned} F_{\text{comb.}}(\varphi_{kh}) &:= \int_{I \times \Gamma_N} g_N^\theta \varphi^\theta + g_N^Y \varphi^Y \, ds dt + \int_{I \times \Gamma_R} \frac{g_R^\theta}{b_R^\theta} \varphi^\theta + \frac{g_R^Y}{b_R^Y} \varphi^Y \, ds dt \\ &+ (\theta^0, \varphi_{kh,0}^{\theta,-})_H + (Y^0, \varphi_{kh,0}^{Y,-})_H, \end{aligned} \quad (23)$$

with $u_{kh} = (\theta_{kh}, Y_{kh})$ and $\varphi_{kh} = (\varphi_{kh}^\theta, \varphi_{kh}^Y)$.

2.4 Numerical solution

In the algorithmic realization, we notice that the choice of trial and test spaces allow for a decoupling of the temporal discretization into slabs, i.e. slices of the space-time cylinder. In the simplest case a slice just encompasses a single temporal interval, resulting in a sequential time-stepping scheme due to the dG(r) test functions, and therefore effectively yielding classical time discretization schemes. For dG(0) and cG(1), implicit Euler-type and Crank-Nicolson-type schemes are recovered. At each time slab, the spatial problems are solved as described in the following.

For the basic implementation of the (linear) heat equation with a classical DWR error estimator, we refer to the *dwr-diffusion* package [32] and the solvers implemented therein. There, the sparse direct solver UMFPACK [11] is used for the linear equation systems.

For the nonlinear combustion equation we employ a classical Newton-type solver as briefly described in the following. In the space-time setting we have to solve

$$A(u_{kh})(\varphi_{kh}) = 0 \quad \forall \varphi_{kh} \in \tilde{X}_{kh}^{r,s},$$

where u_{kh} is the complete space-time solution over all intervals. Given an initial guess u_{kh}^0 , find the update δu of the linear defect-correction problem for $j = 0, 1, 2, \dots$

$$\begin{aligned} A'_u(u_{kh}^j)(\delta u, \varphi_{kh}) &= -A(u_{kh}^j)(\varphi_{kh}), \\ u_{kh}^{j+1} &= u_{kh}^j + \alpha \delta u, \quad \alpha \in (0, 1]. \end{aligned} \tag{24}$$

Remark 2.4. *As we have discontinuous test functions the nonlinear problem can be decoupled into one subproblem per time interval. Then, we obtain a time-stepping scheme with one Newton loop per interval.*

The defect-correction problems are solved using the parallel sparse direct solver MUMPS [1]. The Jacobian $A'(\cdot)(\cdot, \cdot)$ is derived by using analytical expressions, e.g., [64, Chapter 13], in order to maintain superlinear (or quadratic) convergence. However, for $j > 0$ reassembly of the matrix is omitted if the relative reduction of the residual is below a certain threshold. This simplified Newton approach saves a lot of computational time as the factorization only needs to be done after a reassembly step. The step size α is determined by a damping line-search after solving the defect-correction problem.

3 The dual weighted residual method in a space-time setting

In this section, we review the general ideas of the DWR method. We then derive joint and split error identities and corresponding error estimators. Finally, employing a space-time saturation assumption, we derive two-sided estimates.

3.1 Error representation and estimation

For a given goal functional $J(u)$ we want to solve the following optimization problem

$$\min_{u \in X} J(u) \quad s.t. \quad A(u)(\varphi) = F(\varphi) \quad \forall \varphi \in X.$$

Using the method of Lagrange multipliers for this constraint optimization problem (see e.g., [8]) and introducing the dual variable z we obtain the adjoint problem: Find $z \in X$ such that

$$A'_u(u)(\psi, z) = J'_u(u)(\psi) \quad \forall \psi \in X. \quad (25)$$

Remark 3.1. For linear PDEs and linear goal functionals $A'(u)(\psi, z) = A(\psi, z)$ and $J'_u(u)(\psi) = J(\psi)$ hold, respectively.

Remark 3.2. Note that the test and trial functions are switched in (25). Accordingly, the temporal derivative is now applied to the test function ψ . To rectify this, we apply integration by parts to the corresponding scalar product:

$$(\psi, -\partial_t z) + (\nabla \psi, \nabla z) + (\psi(T), z(T))_H = J'_u(u)(\psi) + (\psi(T), z^M)_H \quad \forall \psi \in X. \quad (26)$$

The negative sign of the temporal derivative means the adjoint problem has to be solved backwards in time, with an initial value z^M depending on the goal functional.

For linear PDEs and linear goal functionals we obtain the exact error representations (see [8]):

$$J(u) - J(u_{kh}) = F(z - z_{kh}) - A(u_{kh}, z - z_{kh}) \quad (\text{primal error}) \quad (27)$$

$$= J(u - u_{kh}) - A(u - u_{kh}, z_{kh}) \quad (\text{adjoint error}). \quad (28)$$

In the following, we focus on the primal error representation. As we can see we would need both the exact dual solution z and the discrete dual solution z_{kh} . As this is infeasible for complicated problems we use a discrete solution of higher order for z .

In the equal low order approach both primal and adjoint problem are discretized using the same low order elements. The higher order adjoint solution is then obtained by a patch wise reconstruction. This reconstruction is described in detail in [52].

In the mixed order approach the adjoint problem is discretized by higher order elements and the solution is used as the representation of the exact solution. The fully discrete solution is then obtained by interpolation into the lower order space. It is also possible to use different approaches in time and space e.g. discretizing the primal problem with $cG(1)dG(0)$ and the adjoint problem with $cG(2)dG(0)$.

Additionally, (27) can be split into a temporal and a spatial part by introducing the semidiscrete adjoint solution z_k such that

$$J(u) - J(u_{kh}) = J(u) - J(u_k) + J(u_k) - J(u_{kh}) \quad (29)$$

where temporal and spatial errors are given by, respectively,

$$J(u) - J(u_k) = F(z - z_k) - A(u_{kh}, z - z_k), \quad (30)$$

$$J(u_k) - J(u_{kh}) = F(z_k - z_{kh}) - A(u_{kh}, z_k - z_{kh}). \quad (31)$$

That way (30) can be used for temporal refinement and (31) for spatial refinement.

3.2 DWR for nonlinear time dependent problems

3.2.1 Primal and adjoint problem statements

In general the primal problem can be written as follows: Find $u \in X$ such that

$$A(u)(\varphi) = F(\varphi) \quad \forall \varphi \in X, \quad (32)$$

with

$$A(u)(\varphi) := (\partial_t u, \varphi) + \int_0^T \bar{a}(u(t), \varphi(t)) \, dt + (u(0), \varphi(0))_H, \quad (33)$$

where $\bar{a}(u, \varphi)$ is the variational formulation of an elliptic operator and F is defined as in the linear case (12).

Remark 3.3. *We notice that additional terms due to Neumann or Robin boundary conditions would appear inside $\bar{a}(u(t), \varphi(t))$ and/or $F(\cdot)$.*

The left hand side of the adjoint problem (25) in the space-time context explicitly reads as

$$A'_u(u)(\psi, z) := (\psi, -\partial_t z_{kh}) + \int_0^T \bar{a}'_u(u(t))(\psi(t), z(t)) \, dt + (\psi(T), z_{kh}(T))_H. \quad (34)$$

As an example, for the combustion problem described in the Section 2.3 we obtain $F = F_{\text{comb}}$ as well as the operator of the semi-linear form and its directional derivative, respectively,

$$\begin{aligned} \bar{a}(u(t), \varphi(t)) &= (\nabla \theta, \nabla \varphi^\theta)_H + (\nabla Y, \nabla \varphi^Y)_H + (\omega(u), \varphi^Y - \varphi^\theta)_H \\ &\quad + \int_{\Gamma_R} \frac{a_R^\theta}{b_R^\theta} \theta \varphi^\theta + \frac{a_R^Y}{b_R^Y} Y \varphi^Y \, ds, \end{aligned} \quad (35)$$

$$\begin{aligned} \bar{a}'_u(u(t))(\psi, z) &= (\nabla \psi^\theta, \nabla z^\theta)_H + (\nabla \psi^Y, \nabla z^Y)_H + (\omega'_\theta(u)(\psi^\theta), z^Y - z^\theta)_H \\ &\quad + \int_{\Gamma_R} \frac{a_R^\theta}{b_R^\theta} \psi^\theta z^\theta + \frac{a_R^Y}{b_R^Y} \psi^Y z^Y \, ds + (\omega'_Y(u)(\psi^Y), z^Y - z^\theta)_H. \end{aligned} \quad (36)$$

Therein, $\omega'(u)(\psi)$ is the directional derivative of $\omega(u)$ into the direction ψ .

3.2.2 Goal-oriented error representations

As there are two ways to separate the full estimator into parts, we want to use a clear and precise terminology to distinguish between those two.

Firstly, we can separate by the problem residuals we compute. This gives the *primal* and *adjoint/dual* estimators. Oftentimes, the average of those two parts is also called *mixed* estimator instead of *full* estimator.

Secondly, we can split the difference between the exact and the fully discrete solution by introducing the time-discrete solution. Not doing so we will call the resulting estimator the *joint* estimator. If we calculate both the temporal and spatial error estimator, we will call the sum of both the *split* error

estimator. As both separations can be done simultaneously, combined expressions like split primal estimator or joint dual estimator are possible.

For nonlinear problems we obtain the following error representation [8]:

Theorem 3.4 (Joint error identity). *Let the primal problem and adjoint problem be given. Let $(u, z) \in X \times X$, $(u_k, z_k) \in \tilde{X}_k^r \times \tilde{X}_k^r$ and $(u_{kh}, z_{kh}) \in \tilde{X}_{k,h}^{r,s} \times \tilde{X}_{k,h}^{r,s}$. Then, we have the space-time joint error identity*

$$J(u) - J(u_{kh}) = \frac{1}{2}\rho(u_{kh})(z - z_{kh}) + \frac{1}{2}\rho^*(u_{kh}, z_{kh})(u - u_{kh}) + \mathcal{R}_{kh}, \quad (37)$$

with the primal error estimator ρ and the adjoint error estimator ρ^*

$$\begin{aligned} \rho(u_{kh})(z - z_{kh}) &:= F(z - z_{kh}) - A(u_{kh}, z - z_{kh}), \\ \rho^*(u_{kh}, z_{kh})(u - u_{kh}) &:= J'(u_{kh})(u - u_{kh}) - A'_u(u_{kh})(u - u_{kh}, z_{kh}), \end{aligned}$$

as well as a remainder term \mathcal{R}_{kh} of higher order.

Proof. The proof follows the ideas from [52][Theorem 3.2] with the same remark that $\tilde{X}_k^r \not\subset X$, but only $\tilde{X}_k^r \subset X + \tilde{X}_k^r$. \square

Theorem 3.5 (Split error identity). *With the previous assumptions, we have the split error identity*

$$J(u) - J(u_{kh}) = (J(u) - J(u_k)) + (J(u_k) - J(u_{kh})),$$

with

$$\begin{aligned} J(u) - J(u_k) &= \frac{1}{2}\rho(u_k)(z - z_k) + \frac{1}{2}\rho^*(u_k, z_k)(u - u_k) + R_k, \\ J(u_k) - J(u_{kh}) &= \frac{1}{2}\rho(u_{kh})(z_k - z_{kh}) + \frac{1}{2}\rho^*(u_{kh}, z_{kh})(u_k - u_{kh}) + R_h. \end{aligned}$$

Proof. This the proof of [52][Theorem 3.2]. \square

To establish two-sided estimates below, we also need

Proposition 3.6 (Higher-order joint error). *With the previous assumptions, we have the higher-order error identity*

$$\begin{aligned} J(u_{kh}^{r+1,s+1}) - J(u_{kh}) & \\ = \frac{1}{2}\rho(u_{kh})(z_{kh}^{r+1,s+1} - z_{kh}) + \frac{1}{2}\rho^*(u_{kh}, z_{kh})(u_{kh}^{r+1,s+1} - u_{kh}) + \mathcal{R}_{kh}. & \end{aligned} \quad (38)$$

3.2.3 Error estimators

From the previous error identities, we obtain error estimators in four variants. First, we have the full error estimator

$$\eta := \frac{1}{2}\rho(u_{kh})(z - z_{kh}) + \frac{1}{2}\rho^*(u_{kh}, z_{kh})(u - u_{kh}) + \mathcal{R}_{kh}. \quad (39)$$

However, the unknown solutions u and z still enter. To this end, higher-order approximations $\tilde{u} \in X$ and $\tilde{z} \in X$ are introduced [8]. Examples of such approximations are $\tilde{u} := u_{kh}^{r+1,s+1}$ and $\tilde{z} := z_{kh}^{r+1,s+1}$ such that we obtain the computable error estimator

$$\eta^{(r+1,s+1)} := \frac{1}{2}\rho(u_{kh})(z_{kh}^{r+1,s+1} - z_{kh}) + \frac{1}{2}\rho^*(u_{kh}, z_{kh})(u_{kh}^{r+1,s+1} - u_{kh}) + \mathcal{R}_{kh}. \quad (40)$$

If the remainder term is omitted (which is indeed usually done in practice) we obtain the practical error estimator

$$\eta_h^{(r+1,s+1)} := \frac{1}{2}\rho(u_{kh})(z_{kh}^{r+1,s+1} - z_{kh}) + \frac{1}{2}\rho^*(u_{kh}, z_{kh})(u_{kh}^{r+1,s+1} - u_{kh}). \quad (41)$$

Finally, we also introduce the primal-based error estimator:

$$\eta_{prim}^{(r+1,s+1)} := \rho(u_{kh})(z_{kh}^{r+1,s+1} - z_{kh}). \quad (42)$$

As we also need higher order information of the primal problem for (40) and (41) to calculate the adjoint estimator we now have three possible approaches. In addition to the two previous discretization approaches the equal high order approach uses a higher order element discretization for both the primal and adjoint problem. Then, interpolation into a lower order element space yields both u_{kh} and z_{kh} . However, inserting the interpolated u_{kh} into the goal functional yields worse results compared to a native low order solution, so ideally the primal problem should also be solved in low order to calculate the functional values. Various algorithmic realizations with corresponding theoretical results, and performance analyses for stationary problems were recently established in [16].

3.3 Two-sided estimates

In this section, we show the efficiency and reliability of the computable error estimator $\eta^{(r+1,s+1)}$. To this end, we extend the two-sided error estimates for stationary problems [15, 14] to time-dependent equations in space-time form. Here, slight care must be taken because $\tilde{X}_k^r \not\subset X$, but only $\tilde{X}_k^r \subset X + \tilde{X}_k^r$; see Remark 2.3. We also recall the embeddings noticed in this remark. The prerequisites of primal and adjoint problems and error representations are laid out in the previous subsections. We concentrate on the $cG(s)dG(r)$ discretization in the following.

Lemma 3.7. *Let $u \in X$ be determined by (32) and $z \in X$ be solved by (25). Furthermore, let $\tilde{u} \in X + \tilde{X}_k^{r+1}$ be some approximation, and $u_{kh} \in \tilde{X}_{k,h}^{r,s}$ be the discrete solution, and $u_{kh}^{r+1,s+1} \in \tilde{X}_{k,h}^{r+1,s+1}$ a higher-order discrete solution. Then, it holds*

$$\begin{aligned} |J(u) - J(\tilde{u})| - |J(u) - J(u_{kh}^{r+1,s+1})| &\leq |\eta^{(r+1,s+1)}| \\ &\leq |J(u) - J(\tilde{u})| + |J(u) - J(u_{kh}^{r+1,s+1})|, \end{aligned}$$

where we employ for instance $\tilde{u} := u_{kh}$.

Proof. The first half of the proof is similar to [15]. We start with $\eta = \eta^{(r+1,s+1)} - (\eta^{(r+1,s+1)} - \eta)$ and we have

$$\eta^{(r+1,s+1)} = \eta + (\eta^{(r+1,s+1)} - \eta).$$

From this, we infer

$$\begin{aligned} |\eta^{(r+1,s+1)}| &\leq |\eta| + |\eta - \eta^{(r+1,s+1)}|, \\ |\eta^{(r+1,s+1)}| &\geq |\eta| - |\eta - \eta^{(r+1,s+1)}| \end{aligned}$$

and consequently

$$|\eta| - |\eta - \eta^{(r+1,s+1)}| \leq |\eta^{(r+1,s+1)}| \leq |\eta| + |\eta - \eta^{(r+1,s+1)}|. \quad (43)$$

Now, we employ Remark 2.3 in order to have the correct function space embeddings. By using (37) and (39) as well as (38) and (40), we obtain for $\tilde{u} = u_{kh}$ the identities

$$\begin{aligned} \eta &= J(u) - J(\tilde{u}), \\ \eta^{(r+1,s+1)} &= J(u_{kh}^{r+1,s+1}) - J(\tilde{u}). \end{aligned}$$

Since $\tilde{X}_{k,h}^{r,s} \subset \tilde{X}_{k,h}^{r+1,s+1} \subset \tilde{X}_k^{r+1} \subset X + \tilde{X}_k^{r+1}$, we can subtract and obtain

$$\eta - \eta^{(r+1,s+1)} = J(u) - J(\tilde{u}) - (J(u_{kh}^{r+1,s+1}) - J(\tilde{u})) = J(u) - J(u_{kh}^{r+1,s+1}).$$

Using these last representations and plugging them into (43) shows the assertion. \square

Assumption 1 (Saturation assumption on a space-time goal functional). Let $u_{kh}^{r+1,s+1} \in \tilde{X}_{k,h}^{r+1,s+1}$, $\tilde{u} \in X + \tilde{X}_k^{r+1}$ be some approximation, and $u \in X$. Then, we assume

$$|J(u) - J(u_{kh}^{r+1,s+1})| < b_{kh}|J(u) - J(\tilde{u})|$$

for some $b_{kh} < b_0$ and some fixed $b_0 \in (0, 1)$.

Theorem 3.8. *Let the previous assumptions and prerequisites be fulfilled. Then, the computable error estimator $\eta^{(r+1,s+1)}$ satisfies the following efficiency and reliability estimates:*

$$c_1|\eta^{(r+1,s+1)}| \leq |J(u) - J(\tilde{u})| \leq c_2|\eta^{(r+1,s+1)}| \quad (44)$$

with $c_1 := 1/(1 + b_{kh})$ and $c_2 := 1/(1 - b_{kh})$.

Proof. We start as before with $\eta = \eta^{(r+1,s+1)} - (\eta^{(r+1,s+1)} - \eta)$ and we infer directly

$$\begin{aligned} |\eta| &\leq |\eta^{(r+1,s+1)}| + |\eta^{(r+1,s+1)} - \eta| \\ |\eta| &\geq |\eta^{(r+1,s+1)}| - |\eta^{(r+1,s+1)} - \eta|. \end{aligned}$$

Therefore,

$$|\eta^{(r+1,s+1)}| - |\eta^{(r+1,s+1)} - \eta| \leq |\eta| \leq |\eta^{(r+1,s+1)}| + |\eta^{(r+1,s+1)} - \eta|.$$

With Lemma 3.7 and definitions of the error estimators, it yields

$$|\eta^{(r+1,s+1)}| - |J(u) - J(u_{kh}^{r+1,s+1})| \leq |J(u) - J(\tilde{u})| \leq |\eta^{(r+1,s+1)}| + |J(u) - J(u_{kh}^{r+1,s+1})|.$$

Using the saturation assumption, we obtain

$$|\eta^{(r+1,s+1)}| - \frac{1}{b_{kh}}|J(u) - J(\tilde{u})| < |J(u) - J(\tilde{u})| < |\eta^{(r+1,s+1)}| + b_{kh}|J(u) - J(\tilde{u})|,$$

yielding the desired results and definitions of the constants c_1 and c_2 . \square

Remark 3.9. *Similar results for the $cG(s)cG(r)$ discretization using their corresponding function spaces and embedding can be established in a similar way.*

Remark 3.10. *The previous results can be further refined to the practical error estimator $\eta_h^{(r+1,s+1)}$. In this case, a strengthened saturation assumption is required.*

4 Error localization

Since we want to use the DWR error estimator for grid refinement, we need to split the estimator into element- or DoF-wise error contributions. Three known approaches are the classical integration by parts [8, 4] and a variational filtering operator over patches of elements [10] and a variational partition-of-unity localization [49]. For stationary problems, the effectivity of these localizations was established and numerically substantiated in [49].

First, in Sections 4.1 and 4.2 we derive the variational partition of unity approach for our space-time estimator. Second, Section 4.3 focuses on details of the actual evaluation including the needed interpolation operations. Next, we list in Section 4.4 the resulting error indicators, finally followed by the adaptive algorithms designed in Section 4.5.

4.1 The partition-of-unity approach for the heat equation

In this key section, we extend the ideas from [49] and apply a partition-of-unity (PU) localization to a space-time error estimator. To this end, we first design the PU space. The simplest choice is $V_{PU} = \tilde{X}_{k,h}^{0,1}$, i.e., a $cG(1)dG(0)$ discretization. Effectively, this yields one spatial partition of unity $(\chi_{i,m})_{i=1}^{\#DoFs(\mathcal{T}_h^m)} \in Q_1(\mathcal{T}_h^m)$ per time interval I_m for $m = 1, \dots, M$. As this is a Lagrangian finite element, we have immediately

Proposition 4.1. *For a function $\chi \in V_{PU}$, it holds*

$$\sum_{m=1}^M \sum_{i=1}^{\#DoFs(\mathcal{T}_h^m)} \chi_{i,m} \equiv 1. \quad (45)$$

Remark 4.2. *Since the joint and the split estimators only differ in the interpolation difference we write δz in the following. To obtain the actual estimators one of these identities has to be used*

$$\delta z = \begin{cases} z - z_{kh} & \text{for the joint estimator} \\ z - z_k & \text{for the temporal estimator} \\ z_k - z_{kh} & \text{for the spatial estimator} \end{cases} \quad (46)$$

Inserting the PU into our error estimator, we obtain an error contribution for each spatial DoF $i \in \mathcal{T}_h^m$ on the interval I_m , i.e. the error indicator

$$\begin{aligned} \eta_i^m = & \int_{I_m} \left((f, \delta z \chi_{i,m})_H - (\partial_t u_{kh}, \delta z \chi_{i,m})_H - (\nabla u_{kh}, \nabla(\delta z \chi_{i,m}))_H \right) dt \\ & - ([u_{kh}]_{m-1}, \delta z^+ \chi_{i,m})_H. \end{aligned} \quad (47)$$

Remark 4.3. *Note that we only use the temporal part for marking time steps and calculating the global estimator. Since the indicators for each time step are obtained by summing over all elements in said time step the spatial PU $\chi_{i,m}$ effectively cancels due to the PU property. As a consequence, the spatial PU can be omitted directly in the computation of the temporal indicators.*

For the joint estimator the local contributions are summed over all DoFs of a fixed interval to obtain the corresponding temporal estimator. Subsequent summation over all time intervals yields the global estimator. For the split estimators the spatial estimator is summed over all space-time DoFs and the temporal estimator is summed over all time intervals. The total error estimator is then the sum of these two error parts.

Proposition 4.4 (Primal joint error estimator for the heat equation). *For the space-time formulation of the heat equation, we have the following a posteriori joint error estimator with partition-of-unity localization:*

$$|J(u) - J(u_{kh})| \leq \eta := \sum_m \sum_{i \in \mathcal{T}_h^m} \eta_i^m, \quad (48)$$

with the error indicators

$$\begin{aligned} \eta_i^m := & \int_{I_m} (f, (z - z_{kh})\chi_{i,m})_H \, dt - \int_{I_m} (\nabla u_{kh}, \nabla((z - z_{kh})\chi_{i,m}))_H \, dt \\ & - \int_{I_m} (\partial_t u_{kh}, (z - z_{kh})\chi_{i,m})_H \, dt - ([u_{kh}]_{m-1}, (z^+(t_{m-1}) - z_{kh}^+(t_{m-1}))\chi_{i,m})_H. \end{aligned} \quad (49)$$

Proposition 4.5 (Primal split error estimator for the heat equation). *For the space-time formulation of the heat equation, we have the following a posteriori split error estimator with partition-of-unity localization:*

$$|J(u) - J(u_{kh})| \leq \eta := \sum_m \left(\eta_k^m + \sum_{i \in \mathcal{T}_h^m} \eta_{i,h}^m \right), \quad (50)$$

with the temporal error indicators

$$\begin{aligned} \eta_k^m := & \int_{I_m} \left((f, z - z_k)_H - (\partial_t u_{kh}, z - z_k)_H - (\nabla u_{kh}, \nabla(z - z_k))_H \right) dt \\ & - ([u_{kh}]_{m-1}, z^+(t_{m-1}) - z_k^+(t_{m-1}))_H, \end{aligned} \quad (51)$$

and the spatial error indicators

$$\begin{aligned} \eta_{i,h}^m := & \int_{I_m} (f, (z_k - z_{kh})\chi_{i,m})_H \, dt - \int_{I_m} (\nabla u_{kh}, \nabla((z_k - z_{kh})\chi_{i,m}))_H \, dt \\ & - \int_{I_m} (\partial_t u_{kh}, (z_k - z_{kh})\chi_{i,m})_H \, dt - ([u_{kh}]_{m-1}, (z_k^+(t_{m-1}) - z_{kh}^+(t_{m-1}))\chi_{i,m})_H. \end{aligned} \quad (52)$$

Remark 4.6. *Note that the basis functions are globally defined, so the DoF-wise errors contain an implicit sum over all elements in practice. However, calculating element based estimators by constraining the spatial integrals to each element K yields the unlocalized estimator as the sum over all*

$\chi_{i,m}$ on a single element is 1 and effectively cancels out. To use well-known element based marking strategies the DoF-estimators have to be calculated globally. Afterwards element wise estimators can be calculated by summing all estimators belonging to the DoFs of the corresponding element:

$$\eta_K^m = \sum_{i \in K} \eta_i^m. \quad (53)$$

Proposition 4.7 (Adjoint joint error estimator for the heat equation). *For the space-time formulation of the heat equation, we have the following a posteriori joint error estimator with partition-of-unity localization:*

$$|J(u) - J(u_{kh})| \leq \eta^* := \sum_m \sum_{i \in \mathcal{T}_h^m} \eta_i^{m,*}, \quad (54)$$

with the error indicators

$$\begin{aligned} \eta_i^{m,*} := & \int_{I_m} J'_u(u_{kh})((u - u_{kh})\chi_{i,m}) \, dt - \int_{I_m} (\nabla((u - u_{kh})\chi_{i,m}), \nabla z_{kh})_H \, dt \\ & + \int_{I_m} ((u - u_{kh})\chi_{i,m}, \partial_t z_{kh})_H \, dt + ((u^-(t_m) - u_{kh}^-(t_m))\chi_{i,m}, [z_{kh}]_m)_H. \end{aligned} \quad (55)$$

Proposition 4.8 (Adjoint split error estimator for the heat equation). *For the space-time formulation of the heat equation, we have the following a posteriori split error estimator with partition-of-unity localization:*

$$|J(u) - J(u_{kh})| \leq \eta^* := \sum_m \left(\eta_k^{m,*} + \sum_{i \in \mathcal{T}_h^m} \eta_{i,h}^{m,*} \right), \quad (56)$$

with the temporal error indicators

$$\begin{aligned} \eta_k^{m,*} := & \int_{I_m} \left(J'_u(u_{kh})(u - u_k) + (u - u_k, \partial_t z_{kh})_H - (\nabla(u - u_k), \nabla u_{kh})_H \right) dt \\ & - (u^-(t_m) - u_k^-(t_m), [z_{kh}]_m)_H, \end{aligned} \quad (57)$$

and the spatial error indicators

$$\begin{aligned} \eta_{i,h}^{m,*} := & \int_{I_m} (J'_u(u_{kh})((u_k - u_{kh})\chi_{i,m}) \, dt - \int_{I_m} (\nabla((u_k - u_{kh})\chi_{i,m}), \nabla z_{kh})_H \, dt \\ & + \int_{I_m} ((u_k - u_{kh})\chi_{i,m}, \partial_t z_{kh})_H \, dt - ((u_k^-(t_m) - u_{kh}^-(t_m))\chi_{i,m}, [z_{kh}]_m)_H. \end{aligned} \quad (58)$$

4.2 The partition-of-unity approach for the combustion problem

In this section, we state the error estimator of the combustion problem:

Proposition 4.9 (Primal split error estimator for combustion). *Let us assume homogeneous boundary conditions on Γ_N as well as for the species concentration on Γ_R . For the temperature we have the cooling conditions $\kappa\theta + \partial_n\theta = 0$ on the Robin boundary, such that $g_N^\theta = g_N^Y = g_R^\theta = g_R^Y \equiv 0$, $a_R^\theta = \kappa$, $b_R^\theta = 1$ and $a_R^Y = b_R^Y = 0$ hold. Then, we have the following a posteriori primal split error estimator*

with partition-of-unity localization for the space-time formulation of the time-dependent combustion problem:

$$|J(\{\theta, Y\}) - J(\{\theta, Y\}_{kh})| \leq \eta := \sum_m \left(\eta_k^m + \sum_{i \in \mathcal{T}_h^m} \eta_{i,h}^m \right), \quad (59)$$

with the temporal error indicators

$$\begin{aligned} \eta_k^m = & - \int_{I_m} \left((\partial_t \theta_{kh}, z^\theta - z_k^\theta)_H + (\nabla \theta_{kh}, \nabla (z^\theta - z_k^\theta))_H \right) dt \\ & + \int_{I_m} \int_{\Gamma_R} \kappa \theta (z^\theta - z_k^\theta) ds dt \\ & + \int_{I_m} \left((\partial_t Y_{kh}, z^Y - z_k^Y)_H + (\nabla Y_{kh}, \nabla (z^Y - z_k^Y))_H \right) dt \\ & - \int_{I_m} \left((\omega(\theta_{kh}, Y_{kh}), z^\theta - z_k^\theta)_H + (\omega(\theta_{kh}, Y_{kh}), z^Y - z_k^Y)_H \right) dt \\ & - ([\theta_{kh}]_{m-1}, z^{\theta,+}(t_{m-1}) - z_k^{\theta,+}(t_{m-1}))_H \\ & - ([Y_{kh}]_{m-1}, z^{Y,+}(t_{m-1}) - z_k^{Y,+}(t_{m-1}))_H, \end{aligned} \quad (60)$$

and the spatial error indicators

$$\begin{aligned} \eta_{i,h}^m = & - \int_{I_m} \left((\partial_t \theta_{kh}, (z_k^\theta - z_{kh}^\theta) \chi_{i,m})_H + (\nabla \theta_{kh}, \nabla ((z_k^\theta - z_{kh}^\theta) \chi_{i,m}))_H \right) ds dt \\ & + \int_{I_m} \int_{\Gamma_R} \kappa \theta (z_k^\theta - z_{kh}^\theta) \chi_{i,m} ds dt \\ & + \int_{I_m} \left((\partial_t Y_{kh}, (z_k^Y - z_{kh}^Y) \chi_{i,m})_H + (\nabla Y_{kh}, \nabla ((z_k^Y - z_{kh}^Y) \chi_{i,m}))_H \right) ds dt \\ & - \int_{I_m} \left((\omega(\theta_{kh}, Y_{kh}), (z_k^\theta - z_{kh}^\theta) \chi_{i,m})_H + (\omega(\theta_{kh}, Y_{kh}), (z_k^Y - z_{kh}^Y) \chi_{i,m})_H \right) dt \\ & - ([\theta_{kh}]_{m-1}, (z_k^{\theta,+}(t_{m-1}) - z_{kh}^{\theta,+}(t_{m-1})) \chi_{i,m})_H \\ & - ([Y_{kh}]_{k,m-1}, (z_k^{Y,+}(t_{m-1}) - z_{kh}^{Y,+}(t_{m-1})) \chi_{i,m})_H. \end{aligned} \quad (61)$$

Proposition 4.10 (Adjoint split error estimator for combustion). *Using the same boundary conditions, we have the following a posteriori adjoint split error estimator with partition-of-unity localization for the space-time formulation of the time-dependent combustion problem:*

$$|J(\{\theta, Y\}) - J(\{\theta, Y\}_{kh})| \leq \eta := \sum_m \left[\eta_k^{m,*} + \sum_{i \in \mathcal{T}_h^m} \eta_{i,h}^{m,*} \right], \quad (62)$$

with the temporal error indicators

$$\begin{aligned}
\eta_k^{m,*} = & J'_\theta(\{\theta_{kh}, Y_{kh}\})(\theta - \theta_k)|_{I_m} + J'_Y(\{\theta_{kh}, Y_{kh}\})(Y - Y_k)|_{I_m} \\
& - \int_{I_m} (\theta - \theta_k, -\partial_t z_{kh}^\theta)_H + (\nabla(\theta - \theta_k), \nabla z_{kh}^\theta)_H + \int_{\Gamma_R} \kappa(\theta - \theta_k) z_{kh}^\theta ds dt \\
& - \int_{I_m} (Y - Y_k, \partial_t z_{kh}^Y)_H + (\nabla(Y - Y_k), \nabla z_{kh}^Y)_H dt \\
& - \int_{I_m} (\omega'_\theta(\theta_{kh}, Y_{kh})(\theta - \theta_k) + \omega'_Y(\theta_{kh}, Y_{kh})(Y - Y_k), z_{kh}^Y - z_{kh}^\theta)_H dt \\
& - ((\theta^-(t_m) - \theta_k^-(t_m)), [z_{kh}^\theta]_m) - ((Y^-(t_m) - Y_k^-(t_m)), [z_{kh}^Y]_m),
\end{aligned}$$

and the spatial indicators

$$\begin{aligned}
\eta_{i,h}^{m,*} = & J'_\theta(\{\theta_{kh}, Y_{kh}\})((\theta_k - \theta_{kh})\chi_{i,m})|_{I_m} + J'_Y(\{\theta_{kh}, Y_{kh}\})((Y_k - Y_{kh})\chi_{i,m})|_{I_m} \\
& - \int_{I_m} ((\theta_k - \theta_{kh})\chi_{i,m}, -\partial_t z_{kh}^\theta)_H + (\nabla((\theta_k - \theta_{kh})\chi_{i,m}), \nabla z_{kh}^\theta)_H + \int_{\Gamma_R} \kappa(\theta_k - \theta_{kh})\chi_{i,m} z_{kh}^\theta ds dt \\
& - \int_{I_m} ((Y_k - Y_{kh})\chi_{i,m}, \partial_t z_{kh}^Y)_H + (\nabla((Y_k - Y_{kh})\chi_{i,m}), \nabla z_{kh}^Y)_H dt \\
& - \int_{I_m} (\omega'_\theta((\theta_k - \theta_{kh})\chi_{i,m})(\theta_k - \theta_{kh}) + \omega'_Y(\theta_{kh}, Y_{kh})((Y_k - Y_{kh})\chi_{i,m}), z_{kh}^Y - z_{kh}^\theta)_H dt \\
& - ((\theta_k^-(t_m) - \theta_{kh}^-(t_m))\chi_{i,m}, [z_{kh}^\theta]_m) - ((Y_k^-(t_m) - Y_{kh}^-(t_m))\chi_{i,m}, [z_{kh}^Y]_m).
\end{aligned}$$

4.3 Evaluation of the space-time PU-DWR

For the practical evaluation we need to properly define the interpolation differences. Depending on the approach, we need interpolations from a high order space into a low order space and reconstructions the other way around. In space we denote them as

$$i_h^{(s+1)} : \tilde{X}_{k,h}^{r,s+1} \mapsto \tilde{X}_{k,h}^{r,s} \quad \text{and} \quad i_{2h}^{(s+1)} : \tilde{X}_{k,h}^{r,s} \mapsto \tilde{X}_{k,h}^{r,s+1}.$$

In time we use

$$i_k^{(r+1)} : \tilde{X}_{k,h}^{r+1,s} \mapsto \tilde{X}_{k,h}^{r,s} \quad \text{and} \quad i_{2k}^{(r+1)} : \tilde{X}_{k,h}^{r,s} \mapsto \tilde{X}_{k,h}^{r+1,s}.$$

In the following, we take a closer look at the interpolation difference for a higher order solution as used in the mixed and equal high order approach, i.e. the interpolations $i_h^{(s+1)}$ and $i_k^{(r+1)}$. After that we write down the resulting localized error estimators for each PU-DoF. For good visual representations of the high order reconstructions based on a low order solution see [49] and [52] for the spatial part $i_{2h}^{(s+1)}$ and temporal part $i_{2k}^{(r+1)}$ respectively.

For our visualization the high order space $X_{k,h}^{1,2}$ and the low order space $\tilde{X}_{k,h}^{0,1}$ are used. Then the temporal interpolation operator simplifies to

$$i_k^1 z(t) = \begin{cases} z(t_m) & \text{for } t \in I_m \\ z(t_1) & \text{for } t = 0 \end{cases} \quad (63)$$

For the spatial interpolation operator i_h^2 we use a linear finite element ansatz with the vertex DoFs of the spatial triangulation. Using i_h^2 on the temporally interpolated solution $i_k z$ yields $i_{kh} z$ and vice versa. To illustrate this, Figure 1 shows the different interpolation levels for a single 1+1D finite element.

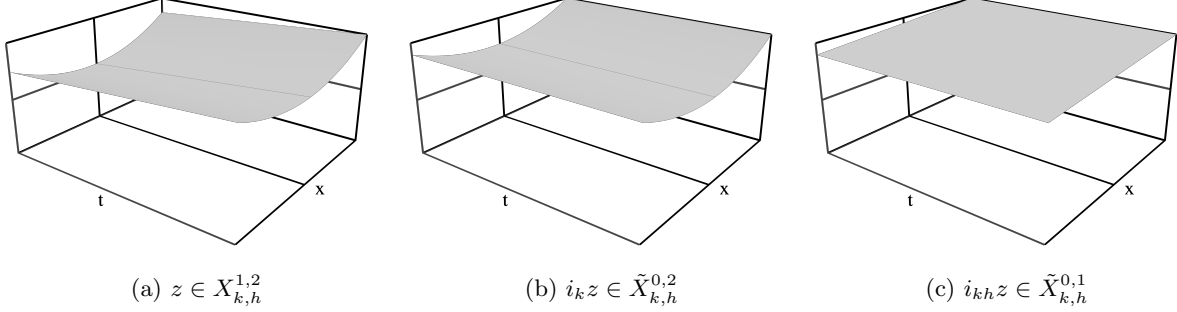


Figure 1: Different interpolation levels on a single 1+1D space-time element

Using these interpolations we can now explicitly evaluate our error estimators. We use $\tilde{X}_{k,h}^{0,1}$ as lower order and $X_{k,h}^{1,2}$ as higher order space. Then u_k and z_k are elements of $\tilde{X}_{k,h}^{0,2}$. Additionally,

$$z|_{I_m}(t) = \frac{t_m - t}{k_m} z_k^{t_{m-1}} + \frac{t - t_{m-1}}{k_m} z_k^{t_m}$$

holds such that evaluation of the primal error estimator on I_m needs the quantities u_{kh} and z_k from I_{m-1} and u_{kh} , z_{kh} and z_k from I_m .

Let \hat{u} and \hat{z} denote the approximated solutions of the primal and adjoint problem. Then we obtain our quantities by the following evaluations:

$$u_{kh}^{t_m} = \begin{cases} \hat{u}^{t_m} & \text{for } \hat{u} \in \tilde{X}_{k,h}^{0,1} \\ i_k^1 \hat{u}^{t_m} & \text{for } \hat{u} \in X_{k,h}^{1,1} \\ i_h^2 \hat{u}^{t_m} & \text{for } \hat{u} \in \tilde{X}_{k,h}^{0,2} \\ i_h^2 i_k^1 \hat{u}^{t_m} & \text{for } \hat{u} \in X_{k,h}^{1,2} \end{cases} \quad (64)$$

$$z_k^{t_m} = \begin{cases} i_{2h}^2 \hat{z}^{t_m} & \text{for } \hat{z} \in \tilde{X}_{k,h}^{0,1} \\ i_k^1 i_{2h}^2 \hat{z}^{t_m} & \text{for } \hat{z} \in X_{k,h}^{1,1} \\ \hat{z}^{t_m} & \text{for } \hat{z} \in \tilde{X}_{k,h}^{0,2} \\ i_k^1 \hat{z}^{t_m} & \text{for } \hat{z} \in X_{k,h}^{1,2} \end{cases} \quad (65)$$

For $z_{kh}^{t_m}$ we have the same interpolations on \hat{z} as for $u_{kh}^{t_m}$ on \hat{u} . For these finite element spaces we can use the midpoint rule with $t_0 = (t_{m+1} - t_m)/2$ for all temporal integrals as the resulting terms are linear time. The only term that might be of higher order is the integration of the right hand side function f for which higher order quadrature rules might have to be used.

Remark 4.11 (Reconstructions for the adjoint estimator). *For the adjoint estimator we additionally need u_k and u . The semi-discrete u_k can be obtained the same way as z_k , but for u we need to change*

the interpolation direction, which results in

$$u|_{I_m}(t) = \frac{t_m - t}{k_m} u_k^{t_m} + \frac{t - t_{m-1}}{k_m} u_k^{t_{m-1}}.$$

4.4 Error indicators in space and time

With the previous evaluations, we can now define the respective indicators in space and time for the heat equation and the combustion problem. Note that the temporal derivative $\partial_t u_{kh}$ vanishes for $u_{kh} \in \tilde{X}_{k,h}^{0,s}$, i.e. piecewise constant elements in time.

Proposition 4.12 (Joint primal error indicator for the heat equation). *We have the following joint error indicator for the heat equation*

$$\begin{aligned} \eta_h^m = & \int_{t_{m-1}}^{t_m} (f(t), (z(t) - z_{kh}^{t_m}) \chi_{i,m})_H dt - (u_{kh}^{t_m} - u_{kh}^{t_{m-1}}, (z_k^{t_{m-1}} - z_{kh}^{t_m}) \chi_{i,m})_H \\ & - \frac{k_m}{2} \cdot (\nabla u_{kh}^{t_m}, (\nabla z_k^{t_{m-1}} + \nabla z_k^{t_m} - 2\nabla z_{kh}^{t_m}) \chi_{i,m} + (z_k^{t_{m-1}} + z_k^{t_m} - 2z_{kh}^{t_m}) \nabla \chi_{i,m})_H \end{aligned} \quad (66)$$

with the time step size $k_m = t_m - t_{m-1}$.

Accordingly, we have

Proposition 4.13 (Split primal error indicators for the heat equation). *The split indicators η_k^m and $\eta_{h,i}^m$ for the heat equation are given by*

$$\begin{aligned} \eta_k^m = & \int_{t_{m-1}}^{t_m} (f(t), (z(t) - z_k^{t_m}))_H dt - k_m/2 \cdot (\nabla u_{kh}^{t_m}, \nabla (z_k^{t_{m-1}} - z_k^{t_m}))_H \\ & - (u_{kh}^{t_m} - u_{kh}^{t_{m-1}}, (z_k^{t_{m-1}} - z_k^{t_m}))_H, \end{aligned} \quad (67)$$

and

$$\begin{aligned} \eta_{h,i}^m = & \int_{t_{m-1}}^{t_m} (f(t), (z_k^{t_m} - z_{kh}^{t_m}) \chi_{i,m})_H dt \\ & - k_m \cdot (\nabla u_{kh}^{t_m}, (\nabla z_k^{t_m} - \nabla z_{kh}^{t_m}) \chi_{i,m} + (z_k^{t_m} - z_{kh}^{t_m}) \nabla \chi_{i,m})_H \\ & - (u_{kh}^{t_m} - u_{kh}^{t_{m-1}}, (z_k^{t_m} - z_{kh}^{t_m}) \chi_{i,m})_H. \end{aligned} \quad (68)$$

Remark 4.14 (Identity of the indicator variants). *Since $\sum_{i \in \mathcal{T}_h^m} \chi_{i,m} \equiv 1$ holds, we obtain*

$$\eta_k^m + \sum_{i \in \mathcal{T}_h^m} \eta_{h,i}^m = \sum_{i \in \mathcal{T}_h^m} \eta_i^m \quad (69)$$

such that the choice between the two indicator variants is only important for adaptive refinement. If one is only interested in estimating the error then both variants are identical.

Using the same interpolations we obtain

Proposition 4.15 (Split primal error indicators for combustion). *For the combustion problem we have the following primal error indicators*

$$\begin{aligned} \eta_k^m = & -k_m/2 \left[(\nabla \theta_{kh}^{t_m}, \nabla (z_k^{\theta, t_{m-1}} - z_k^{\theta, t_m}))_H + \int_{\Gamma_R} \kappa \theta_{kh}^{t_m} (z_k^{\theta, t_{m-1}} - z_k^{\theta, t_m}) ds \right. \\ & (\nabla Y_{kh}^{t_m}, \nabla (z_k^{Y, t_{m-1}} - z_k^{Y, t_m}))_H - (\omega(\theta_{kh}^{t_m}, Y_{kh}^{t_m}), z_k^{\theta, t_{m-1}} - z_k^{\theta, t_m})_H \\ & + (\omega(\theta_{kh}^{t_m}, Y_{kh}^{t_m}), z_k^{Y, t_{m-1}} - z_k^{Y, t_m})_H \left. \right] - (\theta_{kh}^{t_m} - \theta_{kh}^{t_{m-1}}, z_k^{\theta, t_{m-1}} - z_k^{\theta, t_m})_H \\ & - (Y_{kh}^{t_m} - Y_{kh}^{t_{m-1}}, z_k^{Y, t_{m-1}} - z_k^{Y, t_m})_H \end{aligned} \quad (70)$$

and

$$\begin{aligned} \eta_{h,i}^m = & -k_m \left[(\nabla \theta_{kh}^{t_m}, \nabla ((z_k^{\theta, t_m} - z_{kh}^{\theta, t_m}) \chi_{i,m}))_H + \int_{\Gamma_R} \kappa \theta_{kh}^{t_m} (z_k^{\theta, t_m} - z_{kh}^{\theta, t_m}) \chi_{i,m} ds \right. \\ & (\nabla Y_{kh}^{t_m}, \nabla ((z_k^{Y, t_m} - z_{kh}^{Y, t_m}) \chi_{i,m}))_H - (\omega(\theta_{kh}^{t_m}, Y_{kh}^{t_m}), (z_k^{\theta, t_m} - z_{kh}^{\theta, t_m}) \chi_{i,m})_H \\ & + (\omega(\theta_{kh}^{t_m}, Y_{kh}^{t_m}), (z_k^{Y, t_m} - z_{kh}^{Y, t_m}) \chi_{i,m})_H \left. \right] - (\theta_{kh}^{t_m} - \theta_{kh}^{t_{m-1}}, (z_k^{\theta, t_m} - z_{kh}^{\theta, t_m}) \chi_{i,m})_H \\ & - (Y_{kh}^{t_m} - Y_{kh}^{t_{m-1}}, (z_k^{Y, t_m} - z_{kh}^{Y, t_m}) \chi_{i,m})_H. \end{aligned} \quad (71)$$

For the general adjoint estimator we also need z_{kh} and u_k from I_{m+1} which can be obtained by the interpolations described in (64) and (65) respectively. Additionally we only look at goal functionals of the types

$$\begin{aligned} J_1(u)(\varphi) &= \int_0^T (\bar{J}_1(u), \varphi)_H dt \\ J_2(u)(\varphi) &= \int_0^T \int_{\partial\Omega} \bar{J}_2(u) \varphi ds dt \end{aligned}$$

which are essentially interchangeable in the following formulas. Therefore, we only write down the indicators for J_1 .

Proposition 4.16 (Joint adjoint error indicator for the heat equation). *We have the following joint error indicator for the heat equation*

$$\begin{aligned} \eta_i^{m,*} = & \int_{t_{m-1}}^{t_m} J'_u(u_{kh}) ((u(t) - u_{kh}^{t_m}) \chi_{i,m}) dt + ((u_k^{t_{m+1}} - u_{kh}^{t_m}) \chi_{i,m}, z_{kh}^{t_{m+1}} - z_{kh}^{t_m})_H \\ & - \frac{k_m}{2} \cdot ((\nabla u_k^{t_{m+1}} + \nabla u_k^{t_m} - 2\nabla u_{kh}^{t_m}) \chi_{i,m}, \nabla z_{kh}^{t_m})_H. \end{aligned} \quad (72)$$

Proposition 4.17 (Split adjoint error indicators for the heat equation). *The split indicators $\eta_k^{m,*}$ and $\eta_{h,i}^{m,*}$ for the heat equation are given by*

$$\begin{aligned} \eta_k^{m,*} = & \int_{t_{m-1}}^{t_m} J'_u(u_{kh}) (u(t) - u_k^{t_m}) dt - k_m/2 \cdot (\nabla (u_k^{t_{m+1}} - u_k^{t_m}), \nabla z_{kh}^{t_m})_H \\ & + (u_k^{t_{m+1}} - u_k^{t_m}, z_{kh}^{t_{m+1}} - z_{kh}^{t_m})_H, \end{aligned} \quad (73)$$

$$(74)$$

and

$$\begin{aligned}
\eta_{h,i}^{m,*} &= \int_{t_{m-1}}^{t_m} J'_u(u_{kh})((u_k^{t_m} - u_{kh}^{t_m})\chi_{i,m})dt \\
&\quad - k_m \cdot ((\nabla u_k^{t_m} - \nabla u_{kh}^{t_m})\chi_{i,m} + (u_k^{t_m} - u_{kh}^{t_m})\nabla \chi_{i,m}, \nabla z_{kh}^{t_m})_H \\
&\quad + ((u_k^{t_m} - u_{kh}^{t_m})\chi_{i,m}, z_{kh}^{t_{m+1}} - z_{kh}^{t_m})_H.
\end{aligned} \tag{75}$$

All functionals we want to examine for the combustion equation are only dependent on u_{kh} and the primal weight, which is at most linear in time. Therefore, we can simplify the estimator by also applying the midpoint rule to the functional.

Proposition 4.18 (Split adjoint error indicators for combustion). *For the combustion problem we have the following adjoint error indicators*

$$\begin{aligned}
\eta_k^{m,*} &= k_m/2 \left[(J'_{1,\theta}(\theta_{kh}^{t_m}, Y_{kh}^{t_m}), \theta_k^{t_{m+1}} - \theta_k^{t_m})_H + (J'_{1,Y}(\theta_{kh}^{t_m}, Y_{kh}^{t_m}), Y_k^{t_{m+1}} - Y_k^{t_m})_H \right. \\
&\quad - (\nabla(\theta_k^{t_{m+1}} - \theta_k^{t_m}), \nabla z_{kh}^{\theta,t_m})_H - \int_{\Gamma_R} \kappa(\theta_k^{t_{m+1}} - \theta_k^{t_m}) z_{kh}^{\theta,t_m} ds \\
&\quad - (\nabla(Y_k^{t_{m+1}} - Y_k^{t_m}), \nabla z_{kh}^{Y,t_m})_H \\
&\quad \left. - (\omega'_\theta(\theta_{kh}^{t_m}, Y_{kh}^{t_m})(\theta_k^{t_{m+1}} - \theta_k^{t_m}) + (\omega'_Y(\theta_{kh}^{t_m}, Y_{kh}^{t_m})(Y_k^{t_{m+1}} - Y_k^{t_m}), z_{kh}^{Y,t_m} - z_{kh}^{\theta,t_m}) \right] \\
&\quad + (\theta_k^{t_{m+1}} - \theta_k^{t_m}, z_{kh}^{\theta,t_{m+1}} - z_{kh}^{\theta,t_m})_H + (Y_k^{t_{m+1}} - Y_k^{t_m}, z_{kh}^{Y,t_{m+1}} - z_{kh}^{Y,t_m})_H,
\end{aligned} \tag{76}$$

and

$$\begin{aligned}
\eta_{h,i}^{m,*} &= k_m \left[(J'_{1,\theta}(\theta_{kh}^{t_m}, Y_{kh}^{t_m}), (\theta_k^{t_m} - \theta_{kh}^{t_m})\chi_{i,m})_H + (J'_{1,Y}(\theta_{kh}^{t_m}, Y_{kh}^{t_m}), (Y_k^{t_m} - Y_{kh}^{t_m})\chi_{i,m})_H \right. \\
&\quad - (\nabla((\theta_k^{t_m} - \theta_{kh}^{t_m})\chi_{i,m}), \nabla z_{kh}^{\theta,t_m})_H - \int_{\Gamma_R} \kappa(\theta_k^{t_m} - \theta_{kh}^{t_m})\chi_{i,m} z_{kh}^{\theta,t_m} ds \\
&\quad - (\nabla((Y_k^{t_m} - Y_{kh}^{t_m})\chi_{i,m}), \nabla z_{kh}^{Y,t_m})_H \\
&\quad \left. - (\omega'_\theta(\theta_{kh}^{t_m}, Y_{kh}^{t_m})(\theta_k^{t_m} - \theta_{kh}^{t_m})\chi_{i,m} + (\omega'_Y(\theta_{kh}^{t_m}, Y_{kh}^{t_m})(Y_k^{t_m} - Y_{kh}^{t_m})\chi_{i,m}, z_{kh}^{Y,t_m} - z_{kh}^{\theta,t_m}) \right] \\
&\quad + ((\theta_k^{t_m} - \theta_{kh}^{t_m})\chi_{i,m}, z_{kh}^{\theta,t_{m+1}} - z_{kh}^{\theta,t_m}) + ((Y_k^{t_m} - Y_{kh}^{t_m})\chi_{i,m}, z_{kh}^{Y,t_{m+1}} - z_{kh}^{Y,t_m}).
\end{aligned} \tag{77}$$

4.5 Adaptive algorithms

As we have multiple options for solving the primal and adjoint problems, i.e. time-stepping, time-slabbing and fully simultaneous space-time, we firstly present the general algorithm for adaptive refinement. Again, we note that in a space-time context the adjoint problem runs backward in time. Then, all information is collected to evaluate the error estimators. Since one of the error components might dominate, we employ an equilibration for time-stepping and time-slabbing. This will sometimes restrict refinement to space or time, as described in [52]. The overall procedure follows the typical loop: solve, estimate, mark, and refine.

We propose three estimate and three mark and refine procedures, which are summarized in the Algorithms 1,2,3,4,5, and 6.

Algorithm 1 ESTIMATE on a single interval I_m , i.e. time-stepping based

Require: \hat{u} on I_{m-1} and I_m and \hat{z} on I_{m-1} , I_m and I_{m+1}

interpolate/reconstruct u , u_k , u_{kh} as well as z , z_k , z_{kh} at quadrature points.

Calculate η_k^m and $\eta_k^{m,*}$

Calculate $\eta_{h,i}^m$ and $\eta_{h,i}^{m,*}$ for each PU-DoF i on \mathcal{T}_h^m

Algorithm 2 ESTIMATE on a time slab, i.e. $S_m^n: \{I_m, I_{m+1}, I_{m+2}, \dots, I_n\}$

Require: \hat{u} on I_{m-1} and S_m^l and \hat{z} on I_{m-1} , S_m^n and I_{n+1}

interpolate/reconstruct u , u_k , u_{kh} as well as z , z_k , z_{kh} at quadrature points.

Calculate η_k^m to η_k^n and $\eta_k^{m,*}$ to $\eta_k^{n,*}$

Calculate $\eta_{h,i}^m$ to $\eta_{h,i}^n$ and $\eta_{h,i}^{m,*}$ to $\eta_{h,i}^{n,*}$ for each PU-DoF i on $\mathcal{T}_h^m = \mathcal{T}_h^{m+1} = \dots = \mathcal{T}_h^n$

Algorithm 3 ESTIMATE in a fully simultaneous setting

Require: \hat{u} and \hat{z} on the whole space-time cylinder

interpolate/reconstruct u , u_k , u_{kh} as well as z , z_k , z_{kh} at quadrature points.

Calculate $\eta_{k,i}$, $\eta_{k,i}^*$, $\eta_{h,i}$ and $\eta_{h,i}^*$ for each space-time PU-DoF i on \mathcal{T}_{kh}

Algorithm 4 MARK and REFINES for the time-stepping approach

Require: indicators on each interval I_m and equilibration factor $c > 0$

Calculate global temporal estimator $\eta_k = \frac{1}{2} \sum_{m=1}^M (\eta_k^m + \eta_k^{m,*})$

Calculate global spatial estimator $\eta_h = \frac{1}{2} \sum_{m=1}^M \sum_{i \in \mathcal{T}_h^m} (\eta_{h,i}^m + \eta_{h,i}^{m,*})$

if $|\eta_k| * c \geq |\eta_h|$ **then**

mark I_m for temporal refinement based on chosen strategy

end if

if $|\eta_h| * c \geq |\eta_k|$ **then**

for $m = 1, \dots, M$ **do**

mark and refine elements in \mathcal{T}_h^m based on chosen strategy

end for

end if

for $m = 1, \dots, M$ **do**

if I_m is marked **then**

Split/Refine I_m into two intervals with (possibly new) mesh \mathcal{T}_h^m

end if

end for

Algorithm 5 MARK and REFINe for the time-slabbing approach

Require: indicators, equilibration factor $c > 0$ and max. number of intervals per slab N_{\max}

Calculate global temporal estimator $\eta_k = \frac{1}{2} \sum_{m=1}^M (\eta_k^m + \eta_k^{m,*})$

Calculate global spatial estimator $\eta_h = \frac{1}{2} \sum_{m=1}^M \sum_{i \in \mathcal{T}_h^m} (\eta_{h,i}^m + \eta_{h,i}^{m,*})$

if $|\eta_k| * c \geq |\eta_h|$ **then**

mark I_m for temporal refinement based on chosen strategy

end if

if $|\eta_h| * c \geq |\eta_k|$ **then**

for each slab S_m^n **do**

for each PU-DoF $i \in \mathcal{T}_h^m$ **do**

calculate $\eta_{h,i}^{S_m^n} = \frac{1}{2} \sum_{l=m}^n (\eta_{h,i}^l + \eta_{h,i}^{l,*})$

end for

mark and refine elements in \mathcal{T}_h^m based on chosen strategy using indicators $\eta_{h,i}^{S_m^n}$

end for

end if

for each slab S_m^n **do**

for $l = m, \dots, n$ **do**

if I_l is marked **then**

Split/Refine I_l into two intervals

end if

end for

if $n - m > N_{\max}$ **then**

$\hat{n} = \lfloor \frac{m+n}{2} \rfloor$

Split slab S_m^n into two slabs $S_m^{\hat{n}}$ and $S_{\hat{n}+1}^n$

end if

end for

Algorithm 6 MARK and REFINe for the fully simultaneous approach with DoF based marking

Require: indicators on each space-time DoF i and marking parameter $\alpha > 0$

Calculate temporal mean value $\hat{\eta}_k = \frac{1}{2} \sum_{i \in \mathcal{T}_{kh}} (\eta_{k,i} + \eta_{k,i}^*)$

Calculate spatial mean value $\hat{\eta}_h = \frac{1}{2} \sum_{i \in \mathcal{T}_{kh}} (\eta_{h,i} + \eta_{h,i}^*)$

Calculate global spatial estimator $\eta_h = \frac{1}{2} \sum_{m=1}^M \sum_{i \in \mathcal{T}_h^m} (\eta_{h,i}^m + \eta_{h,i}^{m,*})$

for each space-time element $K \in \mathcal{T}_{kh}$ **do**

 calculate $\eta_{k,K} = \frac{1}{2} \sum_{i \in K} (\eta_{k,i} + \eta_{k,i}^*)$

 calculate $\eta_{h,K} = \frac{1}{2} \sum_{i \in K} (\eta_{h,i} + \eta_{h,i}^*)$

if $|\eta_{k,K}| > \alpha |\hat{\eta}_k|$ **then**

 mark K for temporal refinement

end if

if $|\eta_{h,K}| > \alpha |\hat{\eta}_h|$ **then**

 mark K for spatial refinement

end if

end for

refine space-time mesh \mathcal{T}_{kh}

5 Numerical tests

In this final section, we substantiate our space-time error estimators and algorithms with the help of four numerical experiments. The first configuration uses a $1 + 1D$ full space-time solver based only on deal.II [2]. By using a $2D$ triangulation we can allow for hanging nodes in space and time. This configuration is used as a proof of concept for fully anisotropic refinement. In Configuration 2, a $2 + 1D$ heat equation with manufactured solution is considered. This allows us to investigate in detail effectivity indices. Next, in Configuration 3, again a $2 + 1D$ heat equation is utilized, but with a dynamic manufactured solution inspired by Hartmann. In our final configuration, we consider a non-linear coupled problem, namely nonlinear combustion. Therein, very detailed comparisons of different polynomial degrees, primal, adjoint and full estimators are undertaken. The latter computations are based on extensions of the DTM package *dwr-diffusion* [32] which itself is based on deal.II [2].

5.1 Configuration 1: $1+1D$ Heat equation with a full space-time solver

5.1.1 Problem statement

For this configuration we look at two manufactured solutions on a unit-square space-time cylinder i.e. $\Omega = (0, 1) = I$. The two independent solutions are

$$u_1(t, x) = \sin(\pi x)(1 + t) \exp(-t/2), \quad t, x \in (0, 1), \quad (78)$$

$$u_2(t, x) = \sin(\pi x)t(1 - t)^{3/4}, \quad t, x \in (0, 1). \quad (79)$$

5.1.2 Goal functional

For both manufactured solutions we are interested in the L_2 -error as the functional of interest respectively i.e.

$$J(u_{kh}) = \|u - u_{kh}\|_{L_2(\Sigma)} := (u - u_{kh}, u - u_{kh})^{1/2},$$

which is associated to the directional derivative

$$J'_{u_{kh}}(u_{kh})(v) = \frac{(v, u - u_{kh})}{\|u - u_{kh}\|_{L_2(\Sigma)}}.$$

Here, u being either u_1 or u_2 and u_{kh} as the discrete solution based on the corresponding right hand side.

5.1.3 Details on the implemented function spaces

This configuration is implemented as a full space-time 2D problem, such that some details are different to the previous sections. As we have a 2D mesh instead of a tensor product of two 1D meshes, full anisotropic refinement with hanging nodes in space and especially time is possible. Consequently, for the full space-time approach the discretizations and function spaces employed in this first numerical experiment, we notice that instead we have tensor product spaces on (x, t) i.e. $V_{kh}^p = \{v \in Q_p(K_i) | K_i \in \mathcal{T}_{kh}\}$ on a triangulation \mathcal{T}_{kh} of Σ into quadrilateral space-time elements $K_i = \{[x_0^i, x_1^i] \times [t_0^i, t_1^i]\}$. A benefit of this approach is that the implementation does not differ significantly from a stationary 2D PU-DWR code. The main difference lies in correctly splitting the shape function gradient into the temporal and spatial derivative. With these function spaces the simplest choice of PU-space is now $V_{PU} = Q_1(\mathcal{T}_{kh})$, contrary to Section 4. This results in one PU-function per DoF on \mathcal{T}_{kh} and subsequently space-time DoF-based error estimators.

5.1.4 Details on the anisotropic splitting of the estimator

There are two different approaches for anisotropic splitting of the error estimator. The sequential approach where a higher order dual solution $z \in cG(p+1)cG(p+1)$ is first interpolated in time giving $z_k \in cG(p+1)cG(p)$ and the result is then interpolated in space giving $z_{kh} \in cG(p)cG(p)$. The resulting primal error indicators for DoF i then are

$$\eta_{k,i}^{seq.} = F(z - z_k)\chi_i - A(u_{kh}, (z - z_k)\chi_i) \quad (80)$$

$$\eta_{h,i}^{seq.} = F(z_k - z_{kh})\chi_i - A(u_{kh}, (z_k - z_{kh})\chi_i). \quad (81)$$

These interpolations can also be used to calculate the isotropic indicators

$$\eta_{kh,i}^{iso} = F(z - z_{kh}) - A(u_{kh}, (z - z_{kh})\chi_i) \quad (82)$$

The parallel approach is mostly used in stationary problems and was investigated in [48] for DWR methods. There both interpolations are applied to the higher order dual solution z yielding $z_k \in cG(p+1)cG(p)$ and $z_h \in cG(p)cG(p+1)$. The resulting primal error indicators for DoF i then are

$$\eta_{k,i}^{par.} = F(z - z_k)\chi_i - A(u_{kh}, (z - z_k)\chi_i) = \eta_{k,i}^{seq.} \quad (83)$$

$$\eta_{h,i}^{par.} = F(z - z_h)\chi_i - A(u_{kh}, (z - z_h)\chi_i). \quad (84)$$

Using these localized indicators we can calculate the estimators as

$$\eta^{iso} = \sum_{i \in \mathcal{T}_{kh}} \eta_{kh,i}^{iso} \quad (85)$$

$$\eta^{seq.} = \sum_{i \in \mathcal{T}_{kh}} \eta_{k,i}^{seq.} + \eta_{h,i}^{seq.} \quad (86)$$

$$\eta^{par.} = \sum_{i \in \mathcal{T}_{kh}} \eta_{k,i}^{par.} + \eta_{h,i}^{par.} \quad (87)$$

To calculate these estimators we use Algorithm 3. Then we obtain the effectivity indices as

$$I_{eff}^{iso} = \frac{\eta^{iso}}{\|u - u_{kh}\|_{L_2(\Sigma)}}, \quad I_{eff}^{par.} = \frac{\eta^{par.}}{\|u - u_{kh}\|_{L_2(\Sigma)}}, \quad I_{eff}^{seq.} = \frac{\eta^{seq.}}{\|u - u_{kh}\|_{L_2(\Sigma)}} \quad (88)$$

For the adaptive simulations we used Algorithm 6 with $\alpha = 1.1$ and without the adjoint estimators, so $\eta_{k,i}^* \equiv \eta_{k,i}$ and $\eta_{h,i}^* \equiv \eta_{h,i}$. Additionally for the isotropic case $\eta_{k,i} = \eta_{h,i} = \eta_{kh,i}$ is employed.

5.1.5 Discussion of findings for u_1

For u_1 we investigate behaviour of the estimators under uniform refinement in just one of the dimensions as well under fully anisotropic adaptive refinement.

Table 1 shows that for $u_1 \in Q_1(\Sigma)$ all estimators behave well under globally uniform refinement with desirable effectivity. Additionally, we can see that the isotropic estimator has the highest and the sequential estimator has the lowest deviation from the exact error.

Table 1: Section 5.1: Performance of the error estimator under global refinement for u_1 with $p = 1$

dofs	L_2 error	η_{kh}^{iso}	I_{eff}^{iso}	$\eta_{kh}^{seq.}$	$I_{eff}^{seq.}$	$\eta_{kh}^{par.}$	$I_{eff}^{par.}$
81	$1.03e - 02$	$1.15e - 02$	$1.11e + 00$	$1.03e - 02$	$9.95e - 01$	$1.08e - 02$	$1.05e + 00$
289	$2.58e - 03$	$2.88e - 03$	$1.12e + 00$	$2.67e - 03$	$1.04e + 00$	$2.77e - 03$	$1.08e + 00$
1089	$6.45e - 04$	$7.21e - 04$	$1.12e + 00$	$6.77e - 04$	$1.05e + 00$	$6.99e - 04$	$1.08e + 00$
4225	$1.61e - 04$	$1.80e - 04$	$1.12e + 00$	$1.70e - 04$	$1.06e + 00$	$1.75e - 04$	$1.09e + 00$
16641	$4.03e - 05$	$4.51e - 05$	$1.12e + 00$	$4.27e - 05$	$1.06e + 00$	$4.39e - 05$	$1.09e + 00$
66049	$1.01e - 05$	$1.13e - 05$	$1.12e + 00$	$1.07e - 05$	$1.06e + 00$	$1.10e - 05$	$1.09e + 00$
263169	$2.52e - 06$	$2.82e - 06$	$1.12e + 00$	$2.67e - 06$	$1.06e + 00$	$2.75e - 06$	$1.09e + 00$

Table 2 shows that the temporal estimator is nearly independent of spatial refinement as the estimator stays in the same order of magnitude, while the finest spatial estimators are four orders of magnitude lower than the initial ones. Table 3 shows even less dependence of the spatial estimators to temporal refinement. In both cases we can see that the isotropic estimator is dominated by the unrefined part.

Table 2: Section 5.1: Independence of the temporal error estimators under spatial refinement for u_1 with $p = 1$

dofs	η_{kh}^{iso}	$\eta_k^{seq.} = \eta_k^{par.}$	$\eta_h^{seq.}$	$\eta_h^{par.}$
81	$1.15e-02$	$6.00e-04$	$1.09e-02$	$1.14e-02$
153	$2.88e-03$	$3.82e-04$	$2.50e-03$	$2.86e-03$
297	$7.63e-04$	$3.43e-04$	$4.20e-04$	$6.96e-04$
585	$3.11e-04$	$3.36e-04$	$2.54e-05$	$1.45e-04$
1161	$2.61e-04$	$2.96e-04$	$3.56e-05$	$2.47e-05$
2313	$2.60e-04$	$2.72e-04$	$1.14e-05$	$4.84e-06$
4617	$2.61e-04$	$2.64e-04$	$3.03e-06$	$1.11e-06$

Table 3: Section 5.1: Independence of the spatial error estimators under temporal refinement for u_1 with $p = 1$

dofs	η_{kh}^{iso}	$\eta_k^{seq.} = \eta_k^{par.}$	$\eta_h^{seq.}$	$\eta_h^{par.}$
81	$1.15e-02$	$6.00e-04$	$1.09e-02$	$1.14e-02$
153	$1.15e-02$	$1.93e-04$	$1.13e-02$	$1.15e-02$
297	$1.15e-02$	$6.93e-05$	$1.14e-02$	$1.15e-02$
585	$1.15e-02$	$2.73e-05$	$1.15e-02$	$1.15e-02$
1161	$1.15e-02$	$1.13e-05$	$1.15e-02$	$1.15e-02$
2313	$1.15e-02$	$4.57e-06$	$1.15e-02$	$1.15e-02$
4617	$1.15e-02$	$1.69e-06$	$1.15e-02$	$1.15e-02$

Figure 2 shows the L_2 error and resulting effectivity indices under adaptive refinement. We can see that adaptive refinement for the L_2 error performs worse than global refinement. We suppose that, as u_1 is very smooth and regular, adaptive refinement for the L_2 error is simply not advisable in this case. As for effectivity, we can see that the isotropic estimators are closest to the actual error.

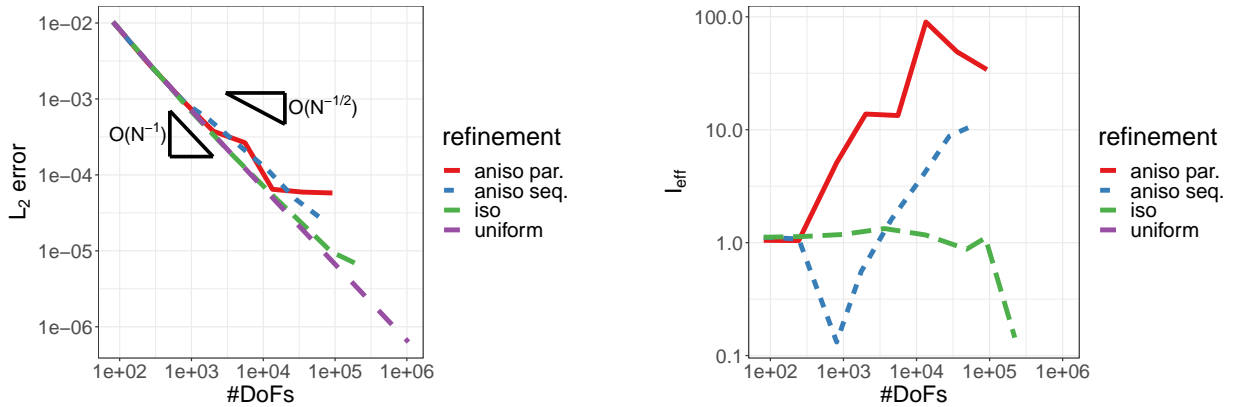


Figure 2: Section 5.1: comparison of L_2 error (left) and I_{eff} (right) for global refinement vs. local refinement using all estimators with $p = 1$

5.1.6 Discussion of findings for u_2

For u_2 we investigate the behaviour for uniform refinement with $p = 1$ compared to $p = 2$ and again investigate fully anisotropic adaptive refinement.

As we are in 2D global h and p refinement of Q_1 elements result in the same number of degrees of freedom. Comparing Tables 4 and 5 we can see that for this problem p refinement performs better than h refinement with a reduction of roughly 78% for higher refinement levels. Comparing the estimators we see that all three approaches work perfectly for bilinear elements. For biquadratic elements both anisotropic estimators outperform the isotropic one with nearly perfect effectivities.

Table 4: Section 5.1: Performance of the error estimator under global refinement for u_2 with $p = 1$

dofs	L_2 error	η_{kh}^{iso}	I_{eff}^{iso}	$\eta_{kh}^{aniso_{seq.}}$	$I_{eff}^{aniso_{seq.}}$	$\eta_{kh}^{aniso_{par.}}$	$I_{eff}^{aniso_{par.}}$
81	$4.45e-03$	$5.27e-03$	$1.18e+00$	$3.92e-03$	$8.81e-01$	$3.39e-03$	$7.63e-01$
289	$2.23e-03$	$2.42e-03$	$1.09e+00$	$2.25e-03$	$1.01e+00$	$2.18e-03$	$9.80e-01$
1089	$1.24e-03$	$1.29e-03$	$1.04e+00$	$1.27e-03$	$1.02e+00$	$1.26e-03$	$1.02e+00$
4225	$7.15e-04$	$7.28e-04$	$1.02e+00$	$7.25e-04$	$1.01e+00$	$7.25e-04$	$1.01e+00$
16641	$4.20e-04$	$4.23e-04$	$1.01e+00$	$4.23e-04$	$1.01e+00$	$4.22e-04$	$1.01e+00$
66049	$2.48e-04$	$2.49e-04$	$1.00e+00$	$2.49e-04$	$1.00e+00$	$2.49e-04$	$1.00e+00$
263169	$1.47e-04$	$1.47e-04$	$1.00e+00$	$1.47e-04$	$1.00e+00$	$1.47e-04$	$1.00e+00$

Table 5: Section 5.1: Performance of the error estimator under global refinement for u_2 with $p = 2$

dofs	L_2 error	η_{kh}^{iso}	I_{eff}^{iso}	$\eta_{kh}^{aniso_{seq.}}$	$I_{eff}^{aniso_{seq.}}$	$\eta_{kh}^{aniso_{par.}}$	$I_{eff}^{aniso_{par.}}$
289	$1.61e-03$	$1.53e-03$	$9.46e-01$	$1.57e-03$	$9.73e-01$	$1.56e-03$	$9.68e-01$
1089	$9.38e-04$	$9.02e-04$	$9.62e-01$	$9.42e-04$	$1.00e+00$	$9.40e-04$	$1.00e+00$
4225	$5.52e-04$	$5.36e-04$	$9.71e-01$	$5.60e-04$	$1.01e+00$	$5.59e-04$	$1.01e+00$
16641	$3.27e-04$	$3.19e-04$	$9.76e-01$	$3.33e-04$	$1.02e+00$	$3.32e-04$	$1.02e+00$
66049	$1.94e-04$	$1.90e-04$	$9.78e-01$	$1.98e-04$	$1.02e+00$	$1.98e-04$	$1.02e+00$
263169	$1.15e-04$	$1.13e-04$	$9.79e-01$	$1.17e-04$	$1.02e+00$	$1.17e-04$	$1.02e+00$
1050625	$6.84e-05$	$6.70e-05$	$9.80e-01$	$6.98e-05$	$1.02e+00$	$6.98e-05$	$1.02e+00$

Figure 3 shows the L_2 error and resulting effectivity indices under local refinement. Here, all estimators work better than global refinement with isotropic and sequential estimators performing comparably and slightly better than the parallel approach.

For effectivity, we can again see that the isotropic estimators are closest to the actual error. The sequential estimator also shows reasonable performance, while the parallel estimator shows a large overestimation for the later refinement steps. As the difference in the increase of DoFs between temporal and spatial refinement gets larger for higher dimensional problems the anisotropic refinement might lead to even better results compared to isotropic refinement. From our findings we would advise the sequential splitting of the error components and will do so ourselves for the following configurations.

Figures 4 and 5 show the absolute pointwise errors $e_i = |u_2(t_i, x_i) - u_{kh,i}|$ and corresponding meshes for the second test case with sequential anisotropic refinement. We can clearly see that at the areas with the highest errors the elements are refined isotropically, while areas with more intermediate errors are sometimes refined only in space (horizontal axis) or in time (vertical axis). These plots also explain why the convergence for isotropic and sequential anisotropic estimators are comparable, as the largest errors occur both in space and time.

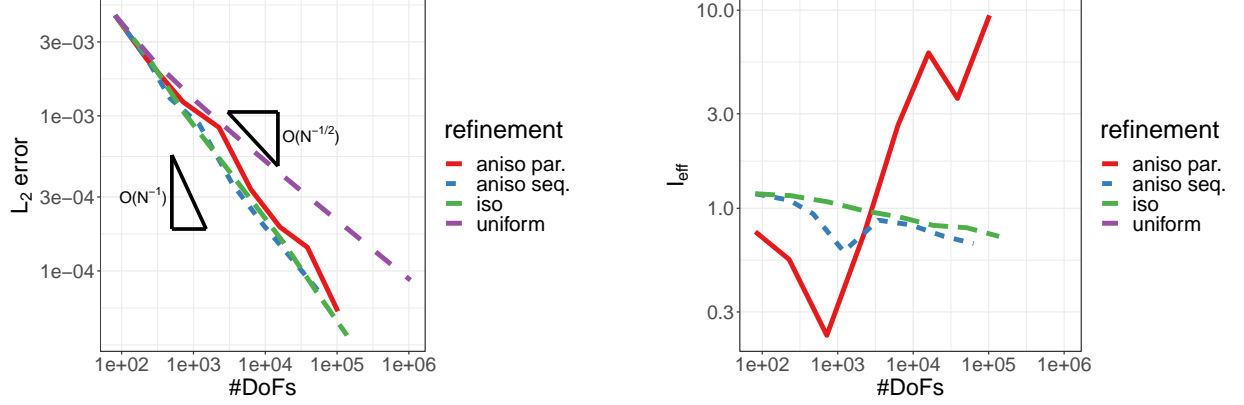


Figure 3: Section 5.1: comparison of L_2 error (left) and I_{eff} (right) for global refinement vs. local refinement using the all estimators with $p = 1$

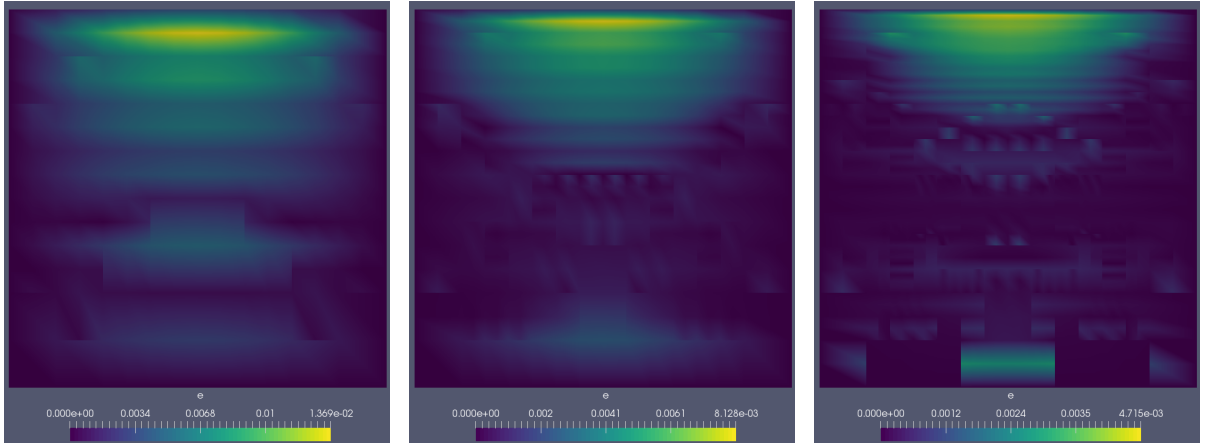


Figure 4: Section 5.1: Absolute pointwise errors for the sequential estimators after 1, 2 and 3 refinement steps.

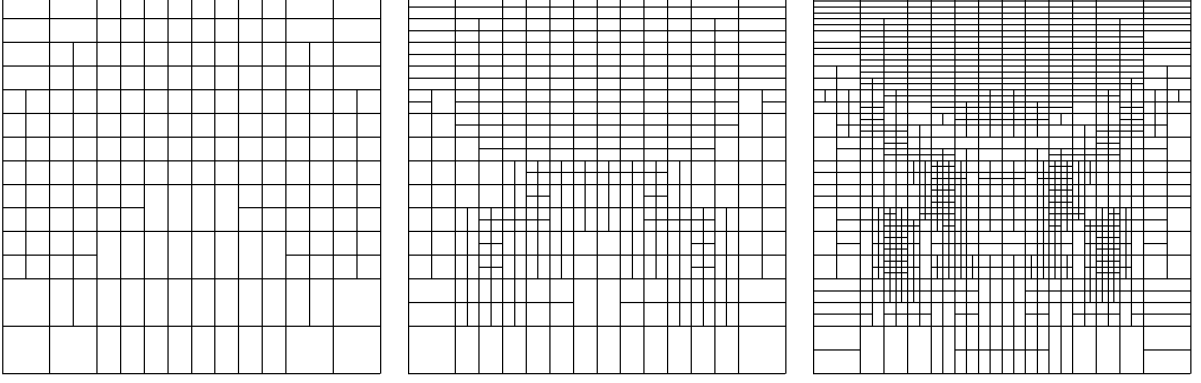


Figure 5: Anisotropic meshes for the sequential estimators after 1, 2 and 3 refinement steps.

Finally, Figure 6 shows the difference between using Q_1 and Q_2 elements for the primal solution. For $p = 1$ the adaptive convergence order is slightly better compared to the $p = 2$ case. But solving this case using $p = 2$ seems more advisable as we get a much better error estimation as the effectivity indices show. We notice that currently in deal.II, hanging node support is not implemented for Q_3 elements under anisotropic refinement. Since this requires extensive implementational work and does not contribute significantly to further insights in this paper, we leave this as future work.

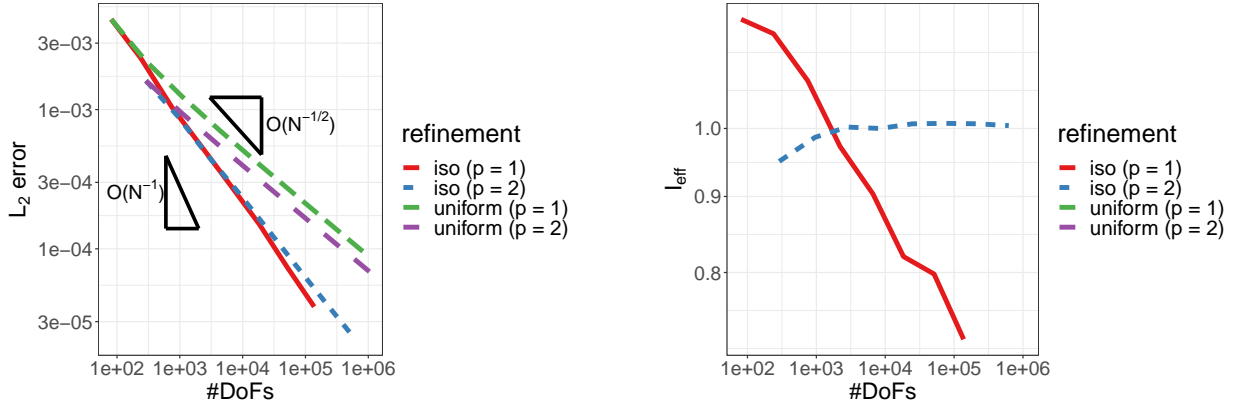


Figure 6: Section 5.1: comparison of L_2 error (left) and I_{eff} (right) for global refinement vs. local refinement using the isotropic estimator for $p = 1$ and $p = 2$

5.2 Configuration 2: 2+1D Heat equation with a simple manufactured solution

5.2.1 Problem statement

To test the 2+1D implementation and the derived estimators we prescribe the following solution for the heat equation introduced in Section 2.2

$$u(t, x, y) = -\frac{(x^2 - x)(y^2 - y)}{4}t. \quad (89)$$

Inserting the solution into the PDE yields the right hand side function

$$f(t, x, y) = -\frac{(x^2 - x)(y^2 - y)}{4} + \frac{(x^2 - x)}{2}t + \frac{(y^2 - y)}{2}t. \quad (90)$$

5.2.2 Configuration

The PDE is solved on the unit square and the temporal interval $(0, 1)$, i.e. $T = 1$. Inserting $x = 0$, $y = 0$ or $t = 0$ yields $u = 0$, resulting in homogeneous Dirichlet boundary conditions and an initial condition of $u^0 \equiv 0$.

5.2.3 Goal functionals

To test whether the error identity holds, we need a linear goal functional. A simple choice is the averaged solution

$$J(u) = \frac{1}{|\Omega|T} \int_0^T \int_{\Omega} u(t, x) dt dx. \quad (91)$$

Inserting the analytical solution for an arbitrary T we obtain

$$J(u) = -\frac{T}{288}, \quad (92)$$

as reference value.

5.2.4 Discussion of findings

We expect (27) and (28) to hold, which is identical to $I_{\text{eff}} = 1$. We observe the effectivity indices for all three approaches in space defined as

$$I_{\text{eff}}^{Y/Z} = \frac{\eta_{kh}^{Y/Z}}{\|u - u_{kh}\|_{L_2(\Sigma)}}$$

with $\eta_{kh}^{Y/Z}$ as the general estimator for $\hat{u}_{kh} \in Y$ and $\hat{z}_{kh} \in Z$ as defined in Propositions 4.13 and 4.17 for the primal and adjoint estimators respectively. All estimators are computed using Algorithm 1.

Tables 6 and 7 show that all approaches yield effectivity indices very close to 1. We also notice, that the biggest difference between primal and adjoint estimator is obtained for the mixed order approach. However, this is not surprising as the approach is tailored to the primal estimator and calculating the adjoint estimator could be seen as questionable for the two following reasons. When interpolating the higher order solution for the adjoint problem for z_{kh} we do not obtain the optimal z_{kh} compared to solving with bilinear elements directly. Additionally, reconstruction the higher order primal solution yields a worse approximation compared to solving directly with biquadratic finite elements.

Furthermore, we notice that we use a lot more elements in time than in space. In space-time the estimator is dependent on a good balance between space and time discretization. For the sake of brevity we investigate this further in the following configuration as the solution is much more interesting.

Table 6: Section 5.2: Performance of the primal error estimators under global refinement for temporal $dG(0)$ discretization of the adjoint equation. Averaged solution functional.

M	N	$I_{\text{eff}}^{cG(1)dG(0)/cG(1)dG(0)}$	$I_{\text{eff}}^{cG(1)dG(0)/cG(2)dG(0)}$	$I_{\text{eff}}^{cG(2)dG(0)/cG(2)dG(0)}$
1000	64	1.008726	1.000479	1.012815
2000	256	1.002999	1.001123	1.004264
4000	1024	1.002757	1.002329	1.003109
8000	4096	1.004806	1.004705	1.004896

Table 7: Section 5.2: Performance of the adjoint error estimators under global refinement for temporal $dG(0)$ discretization of the adjoint equation. Averaged solution functional.

M	N	$I_{\text{eff}}^{cG(1)dG(0)/cG(1)dG(0)}$	$I_{\text{eff}}^{cG(1)dG(0)/cG(2)dG(0)}$	$I_{\text{eff}}^{cG(2)dG(0)/cG(2)dG(0)}$
1000	64	1.018668	1.031224	1.012812
2000	256	1.005793	1.008949	1.004263
4000	1024	1.003508	1.004289	1.003109
8000	4096	1.005001	1.005192	1.004896

5.3 Configuration 3: 2+1D Heat equation with a dynamic manufactured solution

5.3.1 Problem statement

This test case was designed in [26]. We again solve the heat equation. The manufactured solution is a rotating hill on a unit-square spatial domain $\Omega = (0, 1)^2$ in the time interval $(0, T)$, $T = 1$.

The exact solution is given as

$$u(x, y, t) = \frac{1}{1 + (x - x_0(t))^2 + (y - y_0(t))^2} \quad (93)$$

$$x_0(t) = \frac{1}{2} + \frac{1}{4} \cos(2\pi t) \quad (94)$$

$$y_0(t) = \frac{1}{2} + \frac{1}{4} \sin(2\pi t) \quad (95)$$

The right hand side of the problem is obtained as in Section 5.2 by inserting this solution into the heat equation. Additionally, all definitions for $\eta_{kh}^{Y/Z}$ and $I_{\text{eff}}^{Y/Z}$ are the same using again Algorithm 1 to compute the indicators.

5.3.2 Goal functional

Since we are interested in capturing the local behaviour of the solution, we choose the L_2 -error as functional of interest, i.e.

$$J(u_{kh}) = (u - u_{kh}, u - u_{kh})^{1/2}. \quad (96)$$

5.3.3 Comparison of temporal approaches for the adjoint solution

We start by comparing two options for the temporal discretization of the adjoint problem, namely $dG(0)$ (Table 8) and $cG(1)$ (Table 9) elements. The comparisons were done for multiple choices of M_{initial} , but we only included $M_{\text{initial}} = 400$ for the sake of brevity as the results did not differ significantly.

Both for the equal low order and mixed order approach in space we get estimators that are almost independent of the temporal approach. The biggest differences can be seen in the high order approach, but also looking at the effectivity indices the differences are not that significant.

Table 8: Section 5.3: Performance of the primal error estimators under global refinement for temporal $dG(0)$ discretization of the adjoint equation.

M	N	$\eta_{kh}^{cG(1)dG(0)/cG(1)dG(0)}$	$\eta_{kh}^{cG(1)dG(0)/cG(2)dG(0)}$	$\eta_{kh}^{cG(2)dG(0)/cG(2)dG(0)}$
400	64	$5.77335e - 03$	$1.99047e - 02$	$1.77462e - 02$
800	256	$3.30266e - 03$	$5.64178e - 03$	$4.95363e - 03$
1600	1024	$1.10956e - 03$	$1.46754e - 03$	$1.28219e - 03$
3200	4096	$3.13938e - 04$	$3.87165e - 04$	$3.38434e - 04$

Table 9: Section 5.3: Performance of the primal error estimators under global refinement for temporal $cG(1)$ discretization of the adjoint equation.

M	N	$\eta_{kh}^{cG(1)dG(0)/cG(1)cG(1)}$	$\eta_{kh}^{cG(1)dG(0)/cG(2)cG(1)}$	$\eta_{kh}^{cG(2)dG(0)/cG(2)cG(1)}$
400	64	$5.79835e - 03$	$1.99650e - 02$	$1.77902e - 02$
800	256	$3.31318e - 03$	$5.65485e - 03$	$4.96220e - 03$
1600	1024	$1.11250e - 03$	$1.47063e - 03$	$1.28423e - 03$
3200	4096	$3.14708e - 04$	$3.87942e - 04$	$3.38973e - 04$

As the results were comparable, we limit ourselves to a temporal $dG(0)$ discretization for both the primal and adjoint problem.

5.3.4 Comparison of the different spatial approaches

Next we look at the exact error and the resulting estimators for different choices of M_{initial} . We see that the estimators in Tables 10, 11, 12 and 13 are converging to relatively stable values with rising M_{initial} . We can also see that since the temporal elements are only doubled while the spatial elements are quadrupled the initial number of temporal elements has to be large enough for uniform refinement. In adaptive simulations we can control this better as we can choose different fractions of spatial and temporal elements to be marked for refinement.

The equal low order estimators (Table 11) are underestimating the error with an effectivity of roughly $0.34 - 0.40$ for the coarsest mesh. This gets much better after the two refinements where the estimator is close to the exact L_2 -error. However, as the reconstruction effectively works on an even

coarser mesh this is not surprising.

The mixed order estimators (Table 12) are less dependent on the spatial mesh size but overestimate the error with an effectivity of $1.20 - 1.48$. We can also see that the overestimation gets smaller with rising M_{initial} but this is of course an additional cost factor.

The equal high order estimators (Table 13) are also less dependent on the spatial mesh size, but they also use double the amount of degrees of freedom for the primal problem. They also overestimate the error but for large enough M_{initial} the effectivity is less than 1.10. However, Table 14 shows that solving the primal problem with biquadratic elements and using a bilinear interpolation between the vertices does not recover the best approximation u_{kh} . In practice this means that the primal problem should be solved natively

with bilinear elements to obtain the solution for which the error is actually estimated, which leads to additional costs. This gets especially expensive for nonlinear problems. Note that in this particular case the resulting adjoint solution and consequently the estimators would also be different as the L_2 error itself factors into J'_u , so the accuracy of the estimator could be better.

In conclusion both reconstructing a higher order solution and natively solving the primal or adjoint problem with higher order elements in space work well for linear problems, but the reconstructing is cheaper and leads to a better estimator for fine enough meshes.

How the low and mixed order approach perform for higher order finite elements and corresponding errors could be subject of further studies.

Table 10: Section 5.3: The exact L_2 error under global refinement for different initial (uniform) temporal grids and bilinear finite elements in space.

N	$M_{\text{init}} = 100$	$M_{\text{init}} = 400$	$M_{\text{init}} = 800$	$M_{\text{init}} = 1600$
64	$1.68717e - 02$	$1.65372e - 02$	$1.64827e - 02$	$1.64555e - 02$
256	$4.72445e - 03$	$4.51407e - 03$	$4.48052e - 03$	$4.46392e - 03$
1024	$1.28165e - 03$	$1.16287e - 03$	$1.14457e - 03$	$1.13561e - 03$
4096	$3.67307e - 04$	$3.01477e - 04$	$2.91814e - 04$	$2.87159e - 04$

Table 11: Section 5.3: The primal equal low order error estimator under global refinement for different initial (uniform) temporal grids.

N	$M_{\text{init}} = 100$	$M_{\text{init}} = 400$	$M_{\text{init}} = 800$	$M_{\text{init}} = 1600$
64	$6.74336e - 03$	$5.77335e - 03$	$5.65418e - 03$	$5.60003e - 03$
256	$3.66291e - 03$	$3.30266e - 03$	$3.22538e - 03$	$3.18913e - 03$
1024	$1.41226e - 03$	$1.10956e - 03$	$1.06963e - 03$	$1.05100e - 03$
4096	$4.84373e - 04$	$3.13938e - 04$	$2.92451e - 04$	$2.82709e - 04$

Table 12: Section 5.3: The primal mixed order error estimator under global refinement for different initial (uniform) temporal grids.

N	$M_{\text{init}} = 100$	$M_{\text{init}} = 400$	$M_{\text{init}} = 800$	$M_{\text{init}} = 1600$
64	$2.05887e - 02$	$1.99047e - 02$	$1.98049e - 02$	$1.97567e - 02$
256	$6.13544e - 03$	$5.64178e - 03$	$5.57640e - 03$	$5.54573e - 03$
1024	$1.74073e - 03$	$1.46754e - 03$	$1.43250e - 03$	$1.41630e - 03$
4096	$5.44978e - 04$	$3.87165e - 04$	$3.67990e - 04$	$3.59415e - 04$

Table 13: Section 5.3: The primal equal high order error estimator under global refinement for different initial (uniform) temporal grids.

N	$M_{\text{init}} = 100$	$M_{\text{init}} = 400$	$M_{\text{init}} = 800$	$M_{\text{init}} = 1600$
64	$1.82979e - 02$	$1.77462e - 02$	$1.76630e - 02$	$1.76224e - 02$
256	$5.38291e - 03$	$4.95363e - 03$	$4.89527e - 03$	$4.86777e - 03$
1024	$1.52650e - 03$	$1.28219e - 03$	$1.25015e - 03$	$1.23518e - 03$
4096	$4.80895e - 04$	$3.38434e - 04$	$3.20913e - 04$	$3.12975e - 04$

Table 14: Section 5.3: The approximated L_2 error under global refinement for different initial (uniform) temporal grids and biquadratic finite elements in space, where the solution is interpolated down to bilinear elements.

N	$M_{\text{init}} = 100$	$M_{\text{init}} = 400$	$M_{\text{init}} = 800$	$M_{\text{init}} = 1600$
64	$2.16806e - 02$	$2.13230e - 02$	$2.12638e - 02$	$2.12343e - 02$
256	$6.38393e - 03$	$6.17212e - 03$	$6.13780e - 03$	$6.12076e - 03$
1024	$1.72805e - 03$	$1.61279e - 03$	$1.59468e - 03$	$1.58575e - 03$
4096	$4.78600e - 04$	$4.16052e - 04$	$4.06646e - 04$	$4.02072e - 04$

5.3.5 Comparison of adaptive refinement to the original computations

Finally, for this configuration we want to compare our results to those described by Hartmann [26], where the manufactured solution was first formulated. To our knowledge this configuration was not reproduced and published so far, so the original thesis is the only point of comparison. There the classical estimator is used, which is obtained by partial integration to obtain a strong form with jump terms in space.

There, Q_1 elements in space and $dG(0)$ elements in time are used as well, but it is unknown which quadrature formula was used in time for the nonlinear f . We used the right box rule as this is what corresponds to the implicit Euler scheme and got our error ($1.92e - 02$) closest to the error of the original results ($1.75e - 02$).

Table 15 shows the original results, while Tables 16 and 17 show our results with the split and joint

estimators respectively. Even though the marking strategy used by Hartmann is unknown, we got close to the number of temporal elements and the maximum number of spatial elements with fixed rate marking in Algorithm 4. In comparison our estimators better localize the error as we get comparable errors with one less loop that additionally has a smaller maximum number of spatial elements. This can also be seen in Figure 7, where the original results are only performing roughly as well as our computation with uniform refinement, while both PU-DWR estimators yield better convergence. We plotted the L_2 error against the $M * N_{\max}$ which is an upper bound for the actual number of space-time elements as no further information was available from the original computations. However, Table 18 shows that at least for our simulations the actual number is not too far from the upper bound. Additionally, we can see that, as expected, the split estimator outperforms the joint estimator. Finally, Figure 8 shows that the local refinement nicely matches the corresponding solution of Figure 9 and that the meshes are indeed changing over time.

Table 15: Section 5.3: Original results by Hartmann ([26], Table 3.4), with modified notation to match the rest of our present publication.

M	N_{\max}	$\ u - u_{kh}\ _{L_2(\Sigma)}$	η	I_{eff}
16	64	$1.75e - 02$	$7.23e - 02$	4.14
32	124	$1.01e - 02$	$1.65e - 03$	1.63
64	367	$5.35e - 03$	$6.09e - 03$	1.14
128	1195	$2.74e - 03$	$2.90e - 03$	1.06
252	2626	$1.43e - 03$	$1.59e - 03$	1.11
471	5857	$8.15e - 04$	$9.24e - 04$	1.13

Table 16: Section 5.3: Our results with the equal low order primal split PU-DWR estimator with fixed rate marking of 95% in time and 40% in space.

M	N_{\max}	$\ u - u_{kh}\ _{L_2(\Sigma)}$	η	I_{eff}
16	64	$1.92e - 02$	$2.57e - 02$	1.34
32	151	$6.77e - 03$	$7.64e - 03$	1.13
64	364	$2.73e - 03$	$3.32e - 03$	1.22
127	898	$1.26e - 03$	$1.57e - 03$	1.24
250	2110	$6.08e - 04$	$9.24e - 04$	1.52
490	4840	$3.07e - 04$	$6.15e - 04$	2.00

Table 17: Section 5.3: Our results with the equal low order primal joint PU-DWR estimator with fixed rate marking of 95% in time and 40% in space.

M	N_{\max}	$\ u - u_{kh}\ _{L_2(\Sigma)}$	η	I_{eff}
16	64	$1.92e - 02$	$4.15e - 03$	0.22
32	154	$6.67e - 03$	$3.92e - 03$	0.59
64	367	$2.71e - 03$	$3.32e - 03$	1.22
126	859	$1.37e - 03$	$1.60e - 03$	1.17
248	1987	$7.58e - 04$	$9.15e - 04$	1.21
486	4543	$4.27e - 04$	$5.09e - 04$	1.19

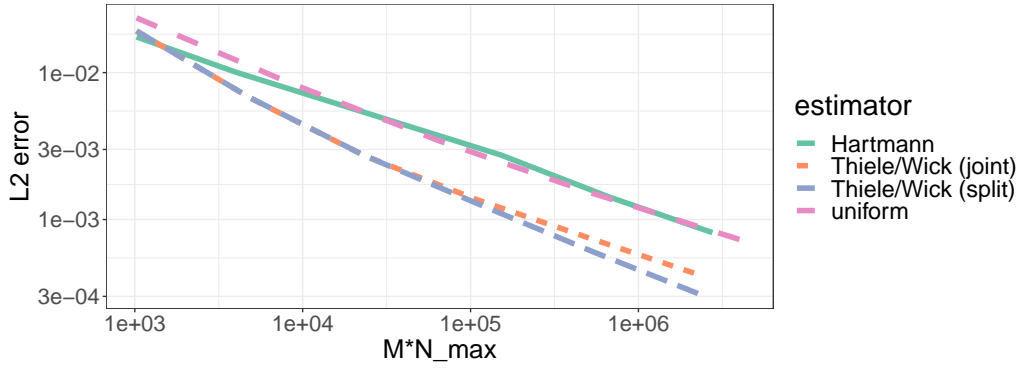


Figure 7: Section 5.3: Error convergence of the Hartmann testcase

Table 18: Section 5.3: Comparison of actual number of space time elements and estimation by $M \cdot N_{\max}$

$loop$	$M * N_{\max}(split)$	$\#elements(split)$	$M * N_{\max}(joint)$	$\#elements(joint)$
0	1024	1024	1024	1024
1	4832	4646	4928	4760
2	23296	21910	23488	22144
3	114046	104962	108234	100512
4	527500	486745	492776	451433
5	2371600	2186416	2207898	1993332

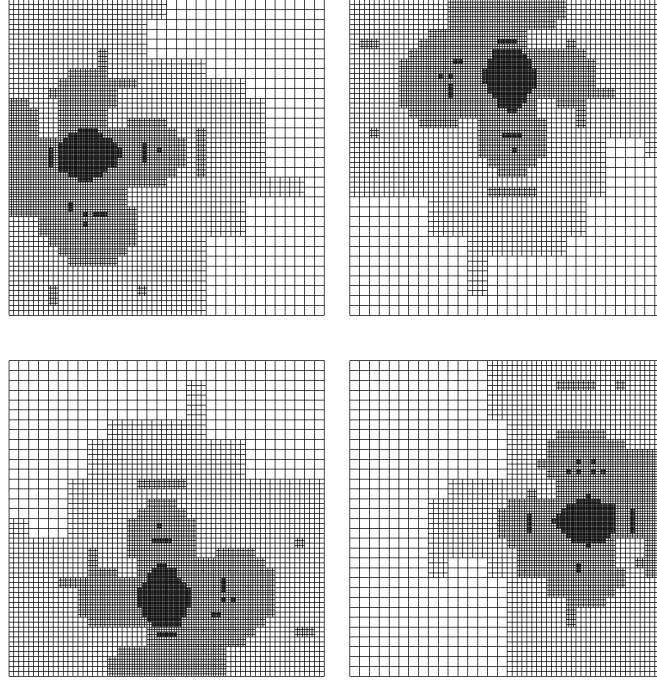


Figure 8: Section 5.3: Grid after 4 refinement loops with the split PU-DWR estimator at $t = i/4$ going counterclockwise from $i = 1$ in the upper right corner to $i = 4$ in the lower right corner.

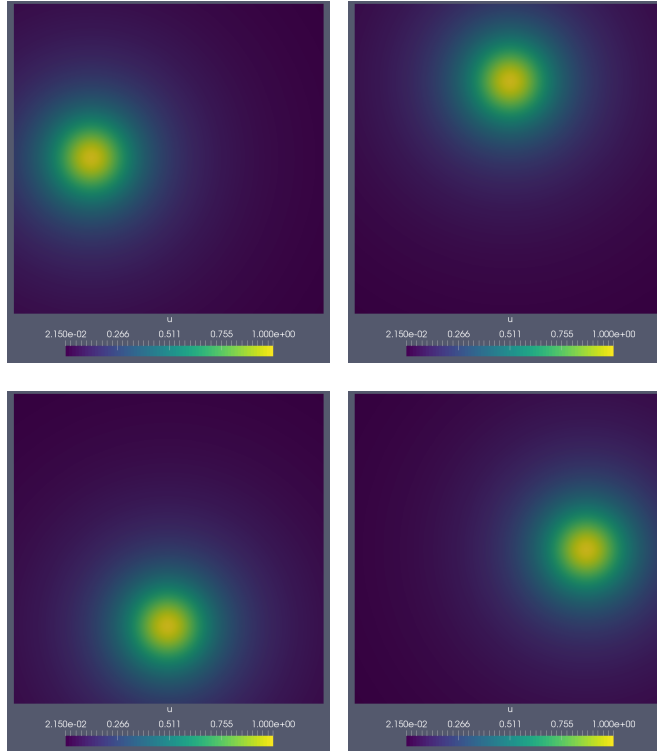


Figure 9: Section 5.3: Solution after 4 refinement loops with the split PU-DWR estimator at $t = i/4$ going counterclockwise from $i = 1$ in the upper right corner to $i = 4$ in the lower right corner.

5.4 Configuration 4: nonlinear combustion

5.4.1 Problem statement

The final test case is as described in [52] (originally based on [33]) and some preliminary results were published in our prior work [60]. Here, we solve the nonlinear combustion equations described in Section 2.3.

5.4.2 Configuration

The reaction is simulated in a rectangular channel of length $L = 60$ and height $H = 16$ in which two cooled rods of length $L/4$ and height $H/4$ are inserted into both channel walls at $L/4$. The reaction is solved for a total of $T = 60$ with 256 time and 896 space DoFs initially.

The cooling of Γ_R is described by the Robin boundary condition $\partial_n \theta = -0.1\theta$, with homogeneous Neumann conditions for the species concentration. The left wall Γ_D is kept at a constant temperature of $\theta_D = 1$ without any combustible species $Y_D = 0$. All other walls Γ_N are described by homogeneous Neumann boundary conditions. An initial flame front is described by

$$\theta^0 = \begin{cases} 1, & x \leq 9 \\ \exp(9 - x), & x > 9 \end{cases} \quad (97)$$

$$Y^0 = \begin{cases} 0, & x \leq 9 \\ 1 - \exp(Le(9 - x)), & x > 9. \end{cases} \quad (98)$$

5.4.3 Parameters

The reaction parameters are a Lewis number of $Le = 1$, a gas expansion of $\alpha = 0.8$ and a dimensionless energy of $\beta = 10$.

5.4.4 Goal Functionals

The first functional we investigate is the average reaction rate i.e.

$$J_1(\theta, Y) = \frac{1}{T|\Omega|} \int_0^T \int_{\Omega} \omega(\theta, Y) dx dt. \quad (99)$$

This nonlinear functional is defined on the whole space-time domain.

For the second functional we calculate the average species concentration on the cooled rods Γ_R i.e.

$$J_2(\theta, Y) = \frac{1}{T|\Gamma_R|} \int_0^T \int_{\Gamma_R} Y ds dt. \quad (100)$$

This is a linear functional, but it is only defined on part the boundary.

5.4.5 Discussion of findings for J_1

For both functionals the indicators for $\eta_{kh}^{Y/Z}$ are computed using Propositions 4.15 and 4.18 and Algorithm 1 with $\hat{u}_{kh} \in Y$ and $\hat{z}_{kh} \in Z$. Then, the full estimators are computed by taking the averages of the primal and adjoint indicators at each space-time Dof and summing over all DoFs.

Tables 19, 20 and 21 show the behaviour of the primal, adjoint and full estimators for J_1 respectively. We can see that all estimators with the mixed order and equal high order approach behave similarly. For both, the adjoint estimator and the resulting full estimator are overestimating the error by about two orders of magnitude. However, the primal estimators are not too far off. The equal low order approach yields the best results on the finest level, and the primal and adjoint estimators are comparable. It can be inferred that there is no benefit from calculating the full estimator in this case. Therefore, we use Algorithm 4 with fixed rate marking refining 50% of all temporal elements and on each interval 30% of all spatial elements based only on the primal indicators. Figure 10 shows the error convergence under adaptive refinement when using only the primal estimator. We can see that for both estimators, the rising number of unknowns, and in the resulting error, our findings for equal low order and mixed order are comparable, and both perform better than global refinement. In Figure 11 the error is plotted with respect to the total number of unknowns needed. In addition to the number of DoFs of the primal problem both the number of Dofs of the adjoint and the PU are taken into account. The low order approach clearly outperforms the mixed order approach. We can also see that the starting disadvantage of having the same error on the coarsest mesh with more DoFs is rectified by the first adaptive refinement step.

Table 19: Section 5.4: Performance of the primal error estimators under global refinement for J_1

M	N	$J(u) - J(u_{kh})$	$\eta_{kh}^{cG(1)/cG(1)}$	$\eta_{kh}^{cG(1)/cG(2)}$	$\eta_{kh}^{cG(2)/cG(2)}$
256	896	$1.08154812e - 02$	$9.99898726e - 04$	$1.54141116e - 03$	$3.73046753e - 03$
512	3584	$2.49545713e - 03$	$5.00929317e - 04$	$1.13434333e - 03$	$1.33777161e - 03$
1024	14366	$5.67139257e - 04$	$2.17940341e - 04$	$5.88255119e - 04$	$5.98302490e - 04$
2048	57344	$1.11745245e - 04$	$8.34682775e - 05$	$3.46300197e - 04$	$3.45416860e - 04$

Table 20: Section 5.4: Performance of the adjoint error estimators under global refinement for J_1

M	N	$J(u) - J(u_{kh})$	$\eta_{kh}^{cG(1)/cG(1)}$	$\eta_{kh}^{cG(1)/cG(2)}$	$\eta_{kh}^{cG(2)/cG(2)}$
256	896	$1.08154812e - 02$	$8.82511469e - 04$	$4.84743239e - 01$	$1.88545655e - 01$
512	3584	$2.49545713e - 03$	$4.48390977e - 04$	$1.99398985e - 01$	$1.28924222e - 01$
1024	14366	$5.67139257e - 04$	$2.11190606e - 04$	$6.62293691e - 02$	$5.78821980e - 02$
2048	57344	$1.11745245e - 04$	$8.29692632e - 05$	$2.08643837e - 02$	$1.99891703e - 02$

Table 21: Section 5.4: Performance of the full error estimators under global refinement for J_1

M	N	$J(u) - J(u_{kh})$	$\eta_{kh}^{cG(1)/cG(1)}$	$\eta_{kh}^{cG(1)/cG(2)}$	$\eta_{kh}^{cG(2)/cG(2)}$
256	896	$1.08154812e - 02$	$9.41205097e - 04$	$2.41600914e - 01$	$9.24075938e - 02$
512	3584	$2.49545713e - 03$	$4.74660147e - 04$	$9.91323210e - 02$	$6.37932253e - 02$
1024	14366	$5.67139257e - 04$	$2.14565473e - 04$	$3.28205570e - 02$	$2.86419478e - 02$
2048	57344	$1.11745245e - 04$	$8.32187704e - 05$	$1.02590417e - 02$	$9.82187670e - 03$

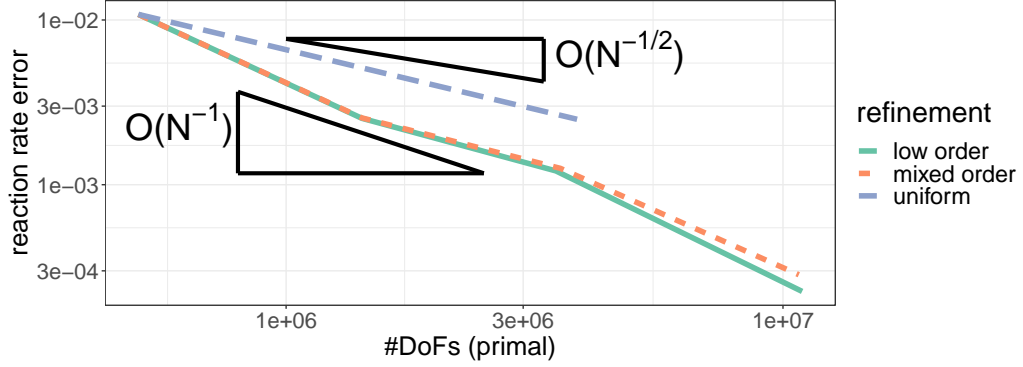


Figure 10: Section 5.4: Error convergence for the reaction rate functional when only counting the number of unknowns for the primal problem.

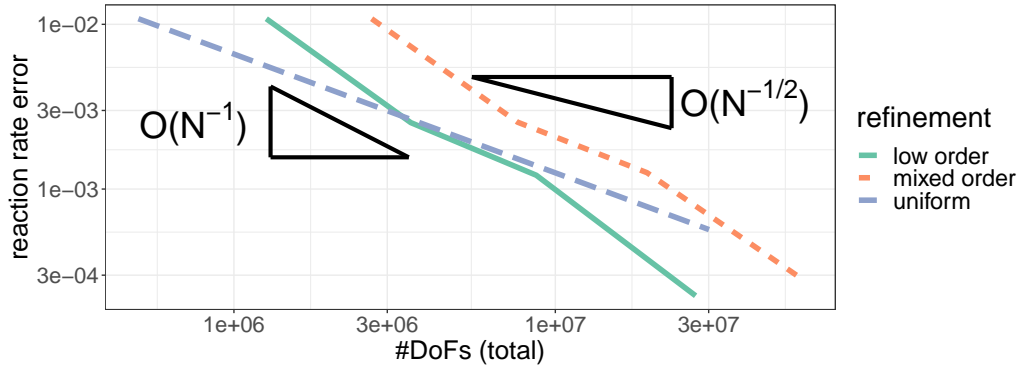


Figure 11: Section 5.4: Error convergence for the reaction rate functional when taking all unknowns into account.

Figures 12, 13, 14, 15, 16 and 17 show the reaction rate and the corresponding grids for three different time points. We can see that the grid evolves nicely and follows the combustion reaction. This shows that our localization works well in capturing the physics and refining accordingly.

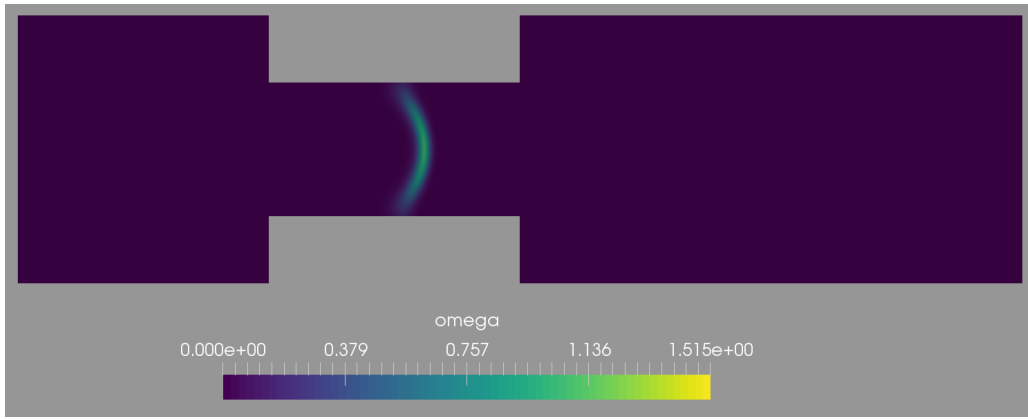


Figure 12: Section 5.4: reaction rate ω at $t = 20$

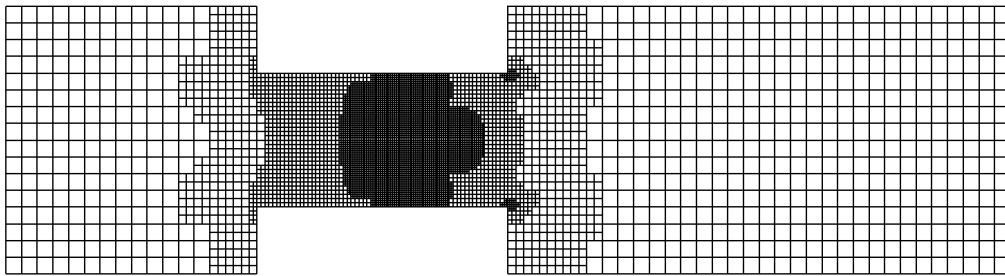


Figure 13: Section 5.4: corresponding grid at $t = 20$

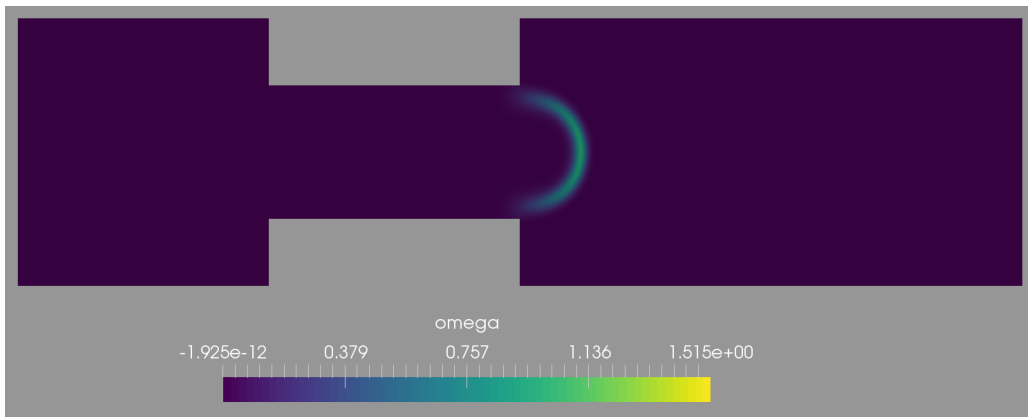


Figure 14: Section 5.4: reaction rate ω at $t = 40$

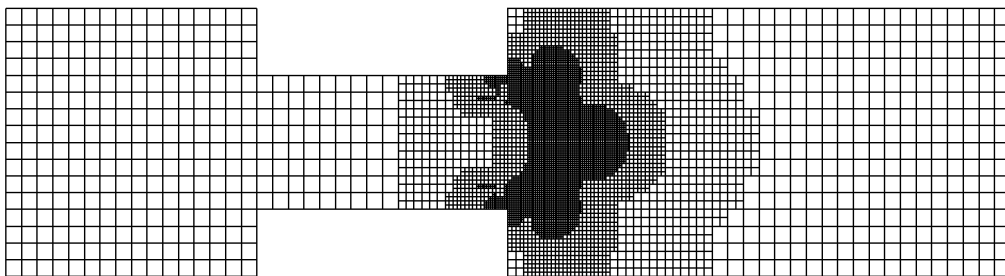


Figure 15: Section 5.4: corresponding grid at $t = 40$

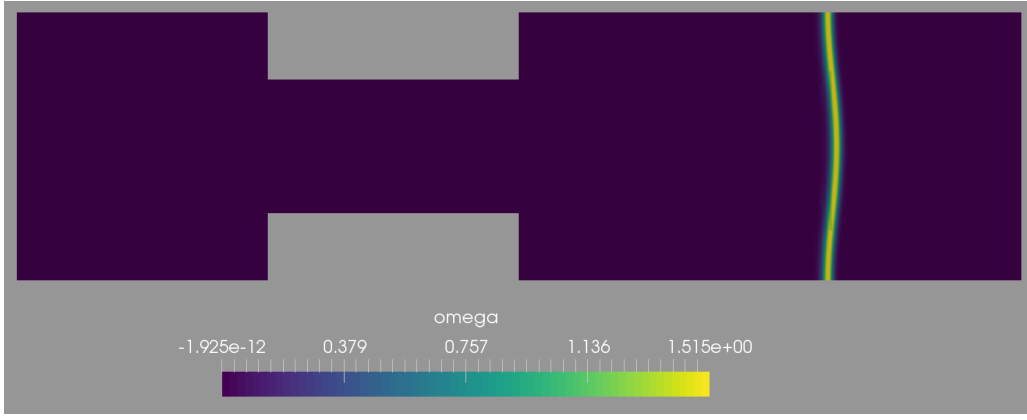


Figure 16: Section 5.4: reaction rate ω at $t = 60$

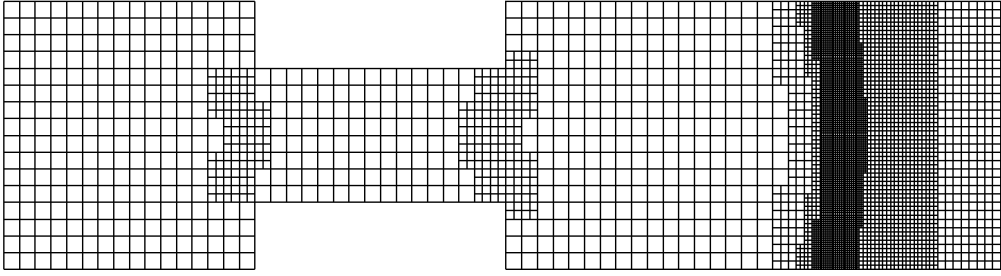


Figure 17: Section 5.4: corresponding grid at $t = 60$

5.4.6 Discussion of findings for J_2

Tables 22, 23 and 24 show the behaviour of the primal, adjoint and full estimators for J_2 respectively. The equal low order approach shows a similar behaviour to the previous functional. However, the overestimation of the adjoint estimators for the mixed order and high order approach is not as bad as for the nonlinear functional. On the other hand their respective primal estimators are underestimating the error by quite a bit. In the full estimators these over- and underestimations are cancelling out quite nicely such that this estimator would be more useful here. For this reason the simulations for Figures 18 and 19 were done by using the full estimator for adaptivity in Algorithm 4 with the same marking strategy as before. As with the first functional we see that both approaches yield comparable results when only counting the memory cost for solving the primal problem. We also see that both approaches eventually outperform uniform refinement when taking the total cost into account. But the equal low order approach is again and still the best choice.

Table 22: Section 5.4: Performance of the primal error estimators under global refinement for J_2

M	N	$J(u) - J(u_{kh})$	$\eta_{kh}^{cG(1)/cG(1)}$	$\eta_{kh}^{cG(1)/cG(2)}$	$\eta_{kh}^{cG(2)/cG(2)}$
256	896	$2.78670640e - 02$	$1.57134836e - 02$	$1.68459624e - 03$	$2.40117972e - 03$
512	3584	$1.29349400e - 02$	$8.36950568e - 03$	$7.70832432e - 04$	$7.82054826e - 04$
1024	14366	$4.17247100e - 03$	$3.88418655e - 03$	$3.57626628e - 04$	$3.52168282e - 04$
2048	57344	$1.07518500e - 03$	$1.63053161e - 03$	$1.77990354e - 04$	$1.76929659e - 04$

Table 23: Section 5.4: Performance of the adjoint error estimators under global refinement for J_2

M	N	$J(u) - J(u_{kh})$	$\eta_{kh}^{cG(1)/cG(1)}$	$\eta_{kh}^{cG(1)/cG(2)}$	$\eta_{kh}^{cG(2)/cG(2)}$
256	896	$2.78670640e - 02$	$1.46726666e - 02$	$1.51762190e - 01$	$6.21329632e - 02$
512	3584	$1.29349400e - 02$	$7.65035908e - 03$	$4.68479946e - 02$	$3.34542288e - 02$
1024	14366	$4.17247100e - 03$	$3.79109953e - 03$	$1.26131290e - 02$	$1.13551533e - 02$
2048	57344	$1.07518500e - 03$	$1.62278719e - 03$	$3.29583742e - 03$	$3.19336781e - 03$

Table 24: Section 5.4: Performance of the full error estimators under global refinement for J_2

M	N	$J(u) - J(u_{kh})$	$\eta_{kh}^{cG(1)/cG(1)}$	$\eta_{kh}^{cG(1)/cG(2)}$	$\eta_{kh}^{cG(2)/cG(2)}$
256	896	$2.78670640e - 02$	$1.51930751e - 02$	$7.53851823e - 02$	$3.12572585e - 02$
512	3584	$1.29349400e - 02$	$8.00993238e - 03$	$2.31194532e - 02$	$1.64872919e - 02$
1024	14366	$4.17247100e - 03$	$3.83764304e - 03$	$6.13512088e - 03$	$5.51198299e - 03$
2048	57344	$1.07518500e - 03$	$1.62665940e - 03$	$1.55892353e - 03$	$1.50821907e - 03$

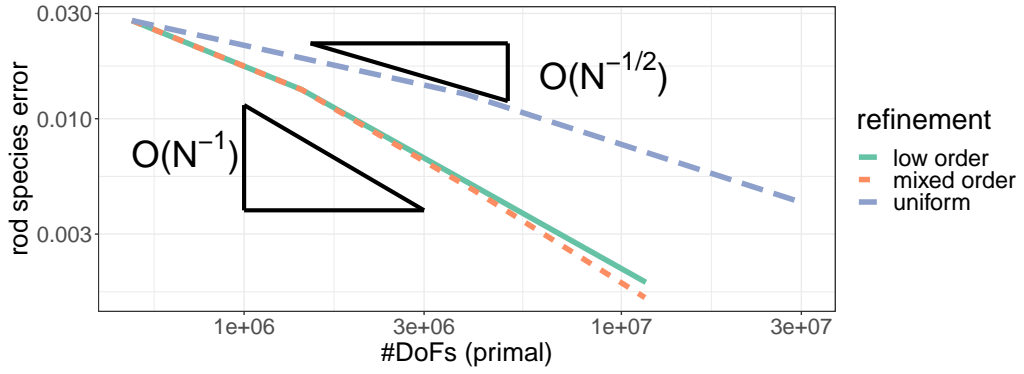


Figure 18: Section 5.4: Error convergence for the species concentration functional when only counting the number of unknowns for the primal problem.

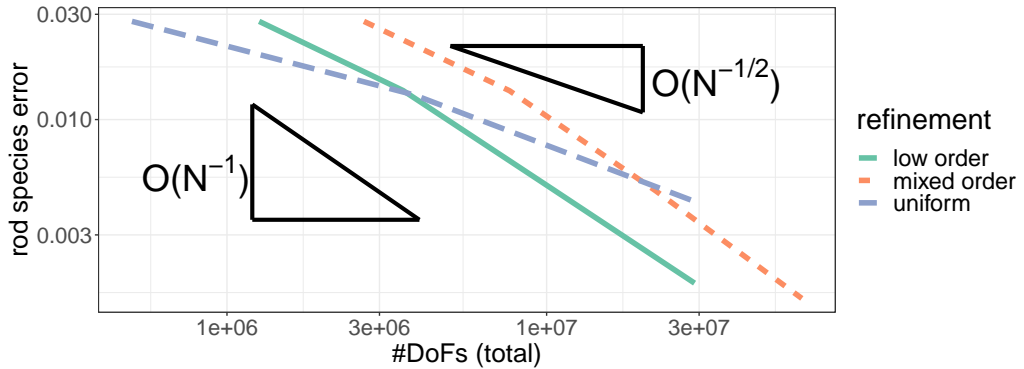


Figure 19: Section 5.4: Error convergence for the species concentration functional when taking all unknowns into account.

Figures 20, 21, 22, 23, 24 and 25 show the species concentration and the refined grids based on J_2 at different time steps. We see that along the cooled rods the grid again follows the combustion

reaction. As that is the area where we have changes in the concentration this fits well. We also see that the mesh is refined around the cooled rod once the reaction moved past them. Together with the convergence behaviour we see again that the novel localization works well.

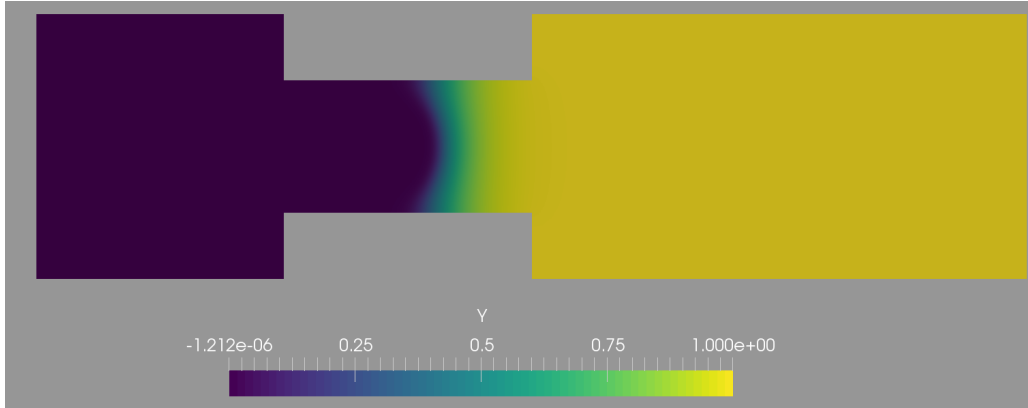


Figure 20: Section 5.4: rod species concentration at $t = 20$

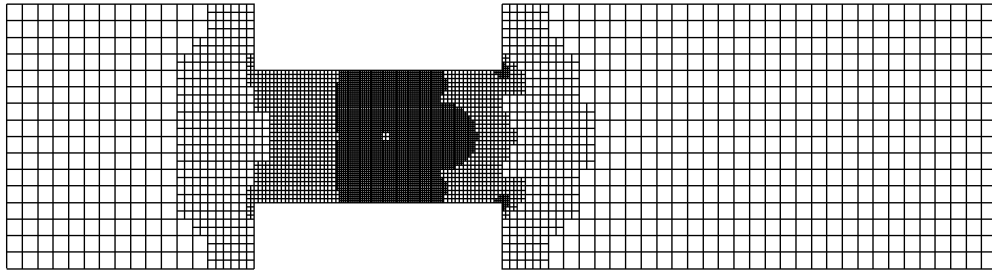


Figure 21: Section 5.4: corresponding grid at $t = 20$

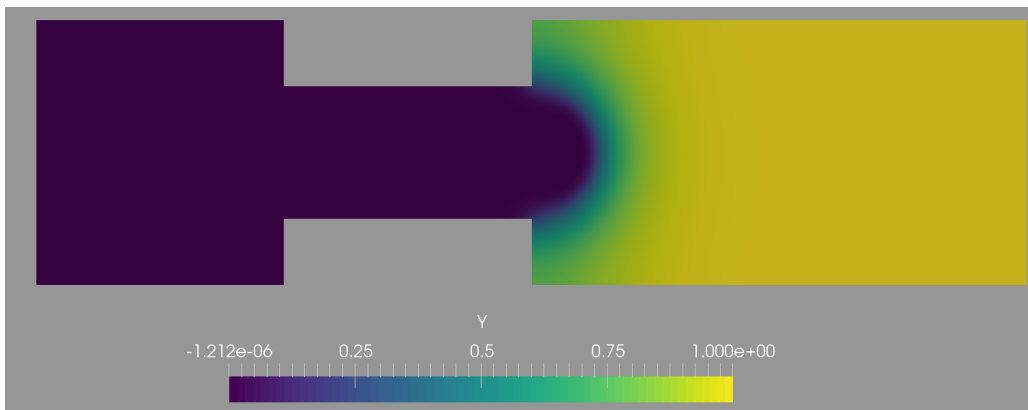


Figure 22: Section 5.4: rod species concentration at $t = 40$

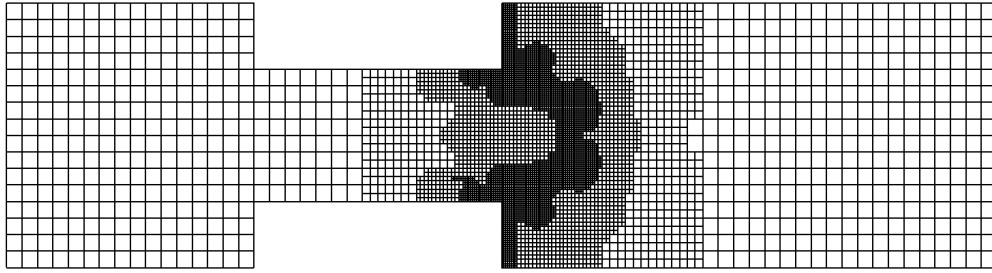


Figure 23: Section 5.4: corresponding grid at $t = 40$

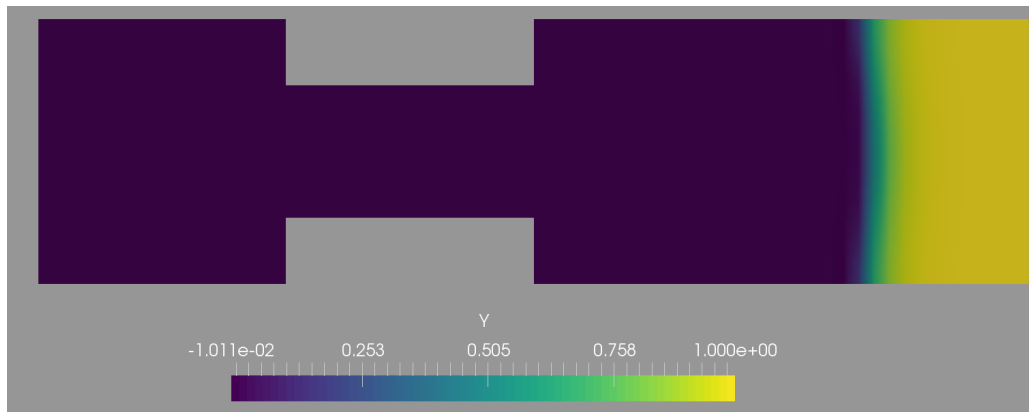


Figure 24: Section 5.4: rod species concentration at $t = 60$

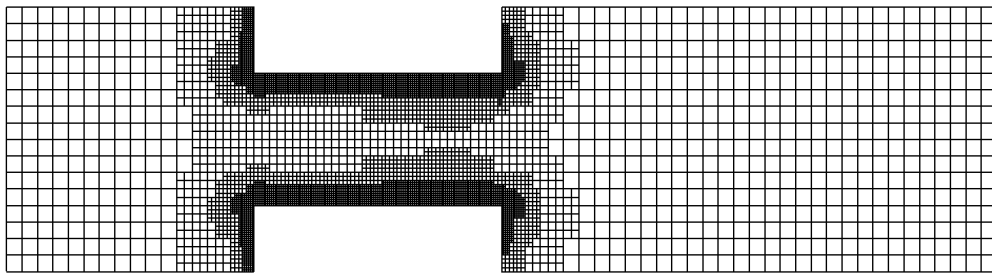


Figure 25: Section 5.4: corresponding grid at $t = 60$

6 Conclusions

In this work, we proposed partition-of-unity (PU) dual-weighted residual a posteriori error estimators and space-time adaptivity for linear and nonlinear partial differential equations. On the theoretical side, we extended two-sided estimates to space-time formulations. From the algorithmic side, the main novelties are the extension of the PU localization to space-time Galerkin finite element discretizations and the realization of split and joint error estimators. From the implementation side, despite starting from pre-implementations in the DTM package *dwr-diffusion* [32] and *deal.II* [2], extensive code developments and debugging was necessary, which greatly exceed existing implementations, specifically for the nonlinear features such as the nonlinear combustion PDE as well as nonlinear goal functionals. In four numerical examples, we studied in the detail the computational performance for the linear heat equation and also for a nonlinear low mach number combustion problem. We also found that the equal low order approach yielded the best estimation and adaptive performance across the board. In ongoing work, we plan to verify our approach for the nonstationary incompressible Navier-Stokes equations and the well-known benchmark problems flow around a cylinder. Furthermore, an example of an immediate practical application of our framework can be found within the excellence cluster PhoenixD¹ in which space-time methods and goal-oriented error estimation are of interest for the efficient solution of multiphysics problems and where the heat equation and the Navier-Stokes equations are needed.

7 Acknowledgments

This work is funded by the Deutsche Forschungsgemeinschaft (DFG) under Germany's Excellence Strategy within the Cluster of Excellence PhoenixD (EXC 2122, Project ID 390833453). The manufactured solutions for configuration 1 were presented at the programming tutorial of the GAMM Juniors Summer School on space-time methods in 2019 (<https://www.gamm-juniors.de/?p=1081>), organized by Philipp Morgenstern (IfAM) and Julia Hauser (TU Graz). Furthermore, the authors thank Uwe Köcher (Hamburg), Julian Roth (IfAM), and Bernhard Endtmayer (IfAM) for fruitful discussions.

References

- [1] P. Amestoy, I. S. Duff, J. Koster, and J.-Y. L'Excellent. A fully asynchronous multifrontal solver using distributed dynamic scheduling. *SIAM Journal on Matrix Analysis and Applications*, 23(1):15–41, 2001.
- [2] D. Arndt, W. Bangerth, B. Blais, T. C. Clevenger, M. Fehling, A. V. Grayver, T. Heister, L. Heltai, M. Kronbichler, M. Maier, P. Munch, J.-P. Pelteret, R. Rastak, I. Tomas, B. Turcksin, Z. Wang, and D. Wells. The *deal.II* library, Version 9.2. *Journal of Numerical Mathematics*, 28(3):131–146, Sept. 2020. Publisher: De Gruyter Section: Journal of Numerical Mathematics.

¹<https://www.phoenixd.uni-hannover.de/>

- [3] W. Bangerth, M. Geiger, and R. Rannacher. Adaptive Galerkin Finite Element Methods for the Wave Equation. *Computational Methods in Applied Mathematics*, 10(1):3–48, Jan. 2010. Publisher: De Gruyter Section: Computational Methods in Applied Mathematics.
- [4] W. Bangerth and R. Rannacher. *Adaptive finite element methods for differential equations*. Lectures in mathematics ETH Zürich. Birkhäuser Verlag, Basel ; Boston, 2003. OCLC: ocm51447498.
- [5] M. Bause, F. A. Radu, and U. Köcher. Space-time finite element approximation of the Biot poroelasticity system with iterative coupling. *Computer Methods in Applied Mechanics and Engineering*, 320:745–768, June 2017.
- [6] R. Becker, D. Meidner, and B. Vexler. Efficient numerical solution of parabolic optimization problems by finite element methods. *Optimization Methods and Software*, 22(5):813–833, Oct. 2007. Publisher: Taylor & Francis _eprint: <https://doi.org/10.1080/10556780701228532>.
- [7] R. Becker and R. Rannacher. Weighted A Posteriori Error Control in FE Methods. page 16, 1996.
- [8] R. Becker and R. Rannacher. An optimal control approach to *a posteriori* error estimation in finite element methods. *Acta Numerica*, 10:1–102, May 2001.
- [9] M. Besier and R. Rannacher. Goal-oriented space-time adaptivity in the finite element Galerkin method for the computation of nonstationary incompressible flow. *International Journal for Numerical Methods in Fluids*, 70(9):1139–1166, 2012. _eprint: <https://onlinelibrary.wiley.com/doi/pdf/10.1002/fld.2735>.
- [10] M. Braack and A. Ern. A Posteriori Control of Modeling Errors and Discretization Errors. *Multiscale Modeling & Simulation*, 1(2):221–238, Jan. 2003. Publisher: Society for Industrial and Applied Mathematics.
- [11] T. A. Davis. Algorithm 832: UMFPACK V4.3—an unsymmetric-pattern multifrontal method. *ACM Transactions on Mathematical Software*, 30(2):196–199, June 2004.
- [12] W. Dörfler, S. Findeisen, and C. Wieners. Space-time discontinuous galerkin discretizations for linear first-order hyperbolic evolution systems. *Computational Methods in Applied Mathematics*, 16(3):409–428, 2016.
- [13] W. Dörfler, C. Wieners, and D. Ziegler. Parallel space-time solutions for the linear visco-acoustic and visco-elastic wave equation. In W. E. Nagel, D. H. Kröner, and M. M. Resch, editors, *High Performance Computing in Science and Engineering '19*, pages 589–599, Cham, 2021. Springer International Publishing.
- [14] B. Endtmayer. *Multi-goal oriented a posteriori error estimates for nonlinear partial differential equations*. PhD thesis, Johannes Kepler University Linz, 2021.

- [15] B. Endtmayer, U. Langer, and T. Wick. Two-Side a Posteriori Error Estimates for the Dual-Weighted Residual Method. *SIAM Journal on Scientific Computing*, 42(1):A371–A394, Jan. 2020. Publisher: Society for Industrial and Applied Mathematics.
- [16] B. Endtmayer, U. Langer, and T. Wick. Reliability and efficiency of DWR-type a posteriori error estimates with smart sensitivity weight recovering. *Computational Methods in Applied Mathematics*, 21(2), 2021.
- [17] K. Eriksson, D. Estep, P. Hansbo, and C. Johnson. *Computational Differential Equations*. Cambridge University Press, 2009. <http://www.csc.kth.se/~jjan/private/cde.pdf>.
- [18] K. Eriksson and C. Johnson. Adaptive Finite Element Methods for Parabolic Problems I: A Linear Model Problem. *SIAM Journal on Numerical Analysis*, 28(1):43–77, 1991.
- [19] K. Eriksson and C. Johnson. Adaptive Finite Element Methods for Parabolic Problems II: Optimal Error Estimates in Linfty L2 and Linfty Linfty. *SIAM Journal on Numerical Analysis*, 32(3):706–740, 1995.
- [20] K. Eriksson, C. Johnson, and A. Logg. *Adaptive Computational Methods for Parabolic Problems*, chapter 24. American Cancer Society, 2004.
- [21] L. Failer. *Optimal Control of Time-Dependent Nonlinear Fluid-Structure Interaction*. PhD thesis, Technical University Munich, 2017.
- [22] L. Failer, D. Meidner, and B. Vexler. Optimal Control of a Linear Unsteady Fluid–Structure Interaction Problem. *Journal of Optimization Theory and Applications*, 170(1):1–27, July 2016.
- [23] L. Failer and T. Wick. Adaptive time-step control for nonlinear fluid–structure interaction. *Journal of Computational Physics*, 366:448–477, Aug. 2018.
- [24] M. J. Gander and M. Neumüller. Analysis of a New Space-Time Parallel Multigrid Algorithm for Parabolic Problems. *SIAM Journal on Scientific Computing*, 38(4):A2173–A2208, Jan. 2016. Publisher: Society for Industrial and Applied Mathematics.
- [25] C. Goll, R. Rannacher, and W. Wollner. The Damped Crank–Nicolson Time-Marching Scheme for the Adaptive Solution of the Black–Scholes Equation. SSRN Scholarly Paper ID 2795622, Social Science Research Network, Rochester, NY, Apr. 2015.
- [26] R. Hartmann. A-posteriori Fehlerschätzung und adaptive Schrittweitein- und Ortsgittersteuerung bei Galerkin-Verfahren für die Wärmeleitungsgleichung. 1998.
- [27] B. Hübner, E. Walhorn, and D. Dinkler. A monolithic approach to fluid–structure interaction using space–time finite elements. *Computer Methods in Applied Mechanics and Engineering*, 193(23):2087–2104, June 2004.

- [28] T. J. R. Hughes and G. M. Hulbert. Space-time finite element methods for elastodynamics: Formulations and error estimates. *Computer Methods in Applied Mechanics and Engineering*, 66(3):339–363, Feb. 1988.
- [29] G. M. Hulbert and T. J. Hughes. Space-time finite element methods for second-order hyperbolic equations. *Computer Methods in Applied Mechanics and Engineering*, 84(3):327–348, 1990.
- [30] D. Khimin, M. C. Steinbach, and T. Wick. Space-time formulation, discretization, and computations for phase-field fracture optimal control problems, 2021.
- [31] U. Köcher. *Variational space-time methods for the elastic wave equation and the diffusion equation*. PhD thesis, Helmut-Schmidt-Universität, 2015.
- [32] U. Köcher, M. P. Bruchhäuser, and M. Bause. Efficient and scalable data structures and algorithms for goal-oriented adaptivity of space-time FEM codes. *SoftwareX*, 10:100239, July 2019.
- [33] J. Lang, editor. *Adaptive Multilevel Solution of Nonlinear Parabolic PDE Systems*. Lecture Notes in Computational Science and Engineering book series (LNCSE, volume 16). Springer, 2001.
- [34] U. Langer and A. Schafelner. Adaptive space-time finite element methods for non-autonomous parabolic problems with distributional sources. *Comput. Methods Appl. Math.*, 2020.
- [35] U. Langer and A. Schafelner. Adaptive space-time finite element methods for parabolic optimal control problems. *Journal of Numerical Mathematics*, 2021.
- [36] U. Langer and A. Schafelner. Space-time hexahedral finite element methods for parabolic evolution problems, 2021. DK Report 2021-05.
- [37] U. Langer and O. Steinbach, editors. *Space-time methods: Application to Partial Differential Equations*. volume 25 of Radon Series on Computational and Applied Mathematics, Berlin. de Gruyter, 2019.
- [38] U. Langer, O. Steinbach, F. Tröltzsch, and H. Yang. Space-Time Finite Element Discretization of Parabolic Optimal Control Problems with Energy Regularization. *SIAM Journal on Numerical Analysis*, 59(2):675–695, Jan. 2021. Publisher: Society for Industrial and Applied Mathematics.
- [39] U. Langer, O. Steinbach, F. Tröltzsch, and H. Yang. Unstructured Space-Time Finite Element Methods for Optimal Control of Parabolic Equations. *SIAM Journal on Scientific Computing*, 43(2):A744–A771, Jan. 2021. Publisher: Society for Industrial and Applied Mathematics.
- [40] D. Meidner. *Adaptive Space-Time Finite Element Methods for Optimization Problems Governed by Nonlinear Parabolic Systems*. Dissertation, 2007.
- [41] D. Meidner and T. Richter. Goal-oriented error estimation for the fractional step theta scheme. *Comput. Methods Appl. Math.*, 14(2):203–230, 2014.

- [42] D. Meidner and T. Richter. A posteriori error estimation for the fractional step theta discretization of the incompressible Navier–Stokes equations. *Computer Methods in Applied Mechanics and Engineering*, 288:45–59, May 2015.
- [43] D. Meidner and B. Vexler. Adaptive Space-Time Finite Element Methods for Parabolic Optimization Problems. *SIAM Journal on Control and Optimization*, 46(1):116–142, Jan. 2007. Publisher: Society for Industrial and Applied Mathematics.
- [44] I. Neitzel and B. Vexler. A priori error estimates for space-time finite element discretization of semilinear parabolic optimal control problems. *Numer. Math.*, 120(2):345–386, 2012.
- [45] M. Neumüller. *Space-time methods fast solvers and applications*. PhD thesis, TU Graz, June 2013.
- [46] J. Oden. A general theory of finite elements II. Applications. *Internat. J. Numer. Methods Engrg.*, 1:247–259, 1969.
- [47] R. Rannacher and F.-T. Suttmeier. A posteriori error estimation and mesh adaptation for finite element models in elasto-plasticity. *Computer Methods in Applied Mechanics and Engineering*, 176(1):333–361, July 1999.
- [48] T. Richter. A posteriori error estimation and anisotropy detection with the dual-weighted residual method. *International journal for numerical methods in fluids*, 62(1):90–118, 2010.
- [49] T. Richter and T. Wick. Variational localizations of the dual weighted residual estimator. *Journal of Computational and Applied Mathematics*, 279:192–208, May 2015.
- [50] A. Schafelner. *Space-time Finite Element Methods*. PhD thesis, Johannes Kepler University Linz, 2022.
- [51] M. Schmich. *Adaptive Finite Element Methods for Computing Nonstationary Incompressible Flows*. PhD thesis, Dec. 2009.
- [52] M. Schmich and B. Vexler. Adaptivity with Dynamic Meshes for Space-Time Finite Element Discretizations of Parabolic Equations. *SIAM Journal on Scientific Computing*, 30(1):369–393, Jan. 2008.
- [53] G. Singh and M. F. Wheeler. A space–time domain decomposition approach using enhanced velocity mixed finite element method. *Journal of Computational Physics*, 374:893–911, 2018.
- [54] O. Steinbach and H. Yang. Comparison of algebraic multigrid methods for an adaptive space–time finite-element discretization of the heat equation in 3D and 4D. *Numerical Linear Algebra with Applications*, 25(3):e2143, 2018. e2143 nla.2143.
- [55] K. Takizawa and T. Tezduyar. Multiscale space–time fluid–structure interaction techniques. *Computational Mechanics*, 48:247–267, 2011.

- [56] T. E. Tezduyar, M. Behr, S. Mittal, and J. Liou. A new strategy for finite element computations involving moving boundaries and interfaces—The deforming-spatial-domain/space-time procedure: II. Computation of free-surface flows, two-liquid flows, and flows with drifting cylinders. *Computer Methods in Applied Mechanics and Engineering*, 94(3):353–371, Feb. 1992.
- [57] T. E. Tezduyar and S. Sathe. Modelling of fluid–structure interactions with the space–time finite elements: Solution techniques. *International Journal for Numerical Methods in Fluids*, 54(6-8):855–900, 2007.
- [58] T. E. Tezduyar, S. Sathe, R. Keedy, and K. Stein. Space–time finite element techniques for computation of fluid–structure interactions. *Computer Methods in Applied Mechanics and Engineering*, 195(17):2002–2027, Mar. 2006.
- [59] T. E. Tezduyar, S. Sathe, and K. Stein. Solution techniques for the fully discretized equations in computation of fluid–structure interactions with the space–time formulations. *Computer Methods in Applied Mechanics and Engineering*, 195(41):5743–5753, Aug. 2006.
- [60] J. P. Thiele and T. Wick. Space-time error control using a partition-of-unity dual-weighted residual method applied to low mach number combustion, 2021.
- [61] J. P. Thiele and T. Wick. Space-time pu-dwr error control and adaptivity for the heat equation. *PAMM*, 21(1):e202100174, 2021.
- [62] R. Verfürth. A posteriori error estimates for finite element discretizations of the heat equation. 40:195–212, 2003.
- [63] T. Wick. On the Adjoint Equation in Fluid-Structure Interaction. WCCM-ECCOMAS2020, 2021.
- [64] T. Wick. Numerical methods for partial differential equations. Hannover : Institutionelles Repository der Leibniz Universität Hannover, DOI: <https://doi.org/10.15488/11709>, January 2022.